Available online at www.sciencedirect.com
ScienceDirect
Precambrian Research 149 (2006) 21–42
Precambrian Research
www.elsevier.com/locate/precamres

The Quetico Intrusions of Western Superior Province: Neo-Archean examples of Alaskan/Ural-type mafic–ultramafic intrusions

Neil T. Pettigrew [1], Kéiko H. Hattori *

Department of Earth Sciences, University of Ottawa, Ontario, Canada K1N 6N5

Received 29 March 2005; received in revised form 5 June 2006; accepted 20 June 2006

Abstract

The Quetico Intrusions are a series of ultramafic–mafic igneous rocks that occur along the northern Quetico subprovince boundary. These intrusions show lithological zoning from cores of olivine-bearing ultramafic rocks to margins of hornblendite and gabbroic rocks, and they are commonly accompanied by Cu–Ni–platinum group element (PGE) sulphide mineralization. We identified three additional Quetico Intrusions in the centre and southern part of the Quetico subprovince, bringing the entire Quetico Intrusion array to be over 125 km in length across the subprovince. The Samuels Lake intrusion in the centre of the subprovince has an U–Pb age of 2688 + 6/−5 Ma, which is similar to the age of ∼2690 Ma for the Quetico Intrusions along the northern subprovince boundary, suggesting that all the Quetico Intrusions are likely to be contemporaneous. The parental magmas of the intrusions were Mg-rich based on the high Mg of olivine and clinopyroxene, and they were hydrous as evidenced by abundant hornblende, early crystallization of clinopyroxene, and the common occurrence of mafic pegmatite. The bulk rocks show arc geochemical signatures, including a high concentration of large ion-lithophile elements combined with a low concentration of high field-strength elements. The mineral compositions of pyroxene and hornblende also plot in the field of arc igneous rocks. The data suggest the derivation of the parental magmas from a mantle wedge or a refractory mantle that was previously metasomatized in a subduction setting.

The Quetico Intrusions display many similarities with Alaskan/Ural-type zoned mafic–ultramafic intrusions along major sutures of Phanerozoic orogenic belts. Common features include their geodynamic settings, internal lithological zoning, mineralogy and mineral chemistry, and common association with PGE mineralization. The striking similarities between the two indicate that the late Archean Quetico Intrusions likely formed in a tectonic setting similar to that of the Alaskan/Ural-type intrusions. We propose that the parental magmas for the Quetico Intrusions formed during the very early stage of accretion of the Wawa arc to the Wabigoon subprovince. Oblique accretion of the Wawa arc likely steepened the subduction angle, which allowed upwelling of hot asthenospheric mantle. This resulted in high degrees of partial melting in the mantle wedge to produce the Quetico Intrusions.

Keywords: Archean cratonization; Accretion; Subduction; Zoned igneous complex; High Mg magma; Arc magmas; Archean tectonics; Oblique accretion; PGE mineralization

1. Introduction

Several mafic–ultramafic intrusions, collectively known as the Quetico Intrusions, occur along the northern boundary of the Quetico metasedimentary subprovince (Figs. 1 and 2). These late Archean intrusions are important in understanding the evolution of this Archean craton because they represent the final mantle-

* Corresponding author. Tel.: +1 613 562 5838; fax: +1 613 562 5192.
E-mail address: khattori@uottawa.ca (K.H. Hattori).
[1] Present address: Precambrian Geoscience Section, Ontario Geological Survey, 933 Ramsey Lake Road, Sudbury, Ontario, Canada P3E 6B5.

0301-9268/$ – see front matter © 2006 Elsevier B.V. All rights reserved.
doi:10.1016/j.precamres.2006.06.004

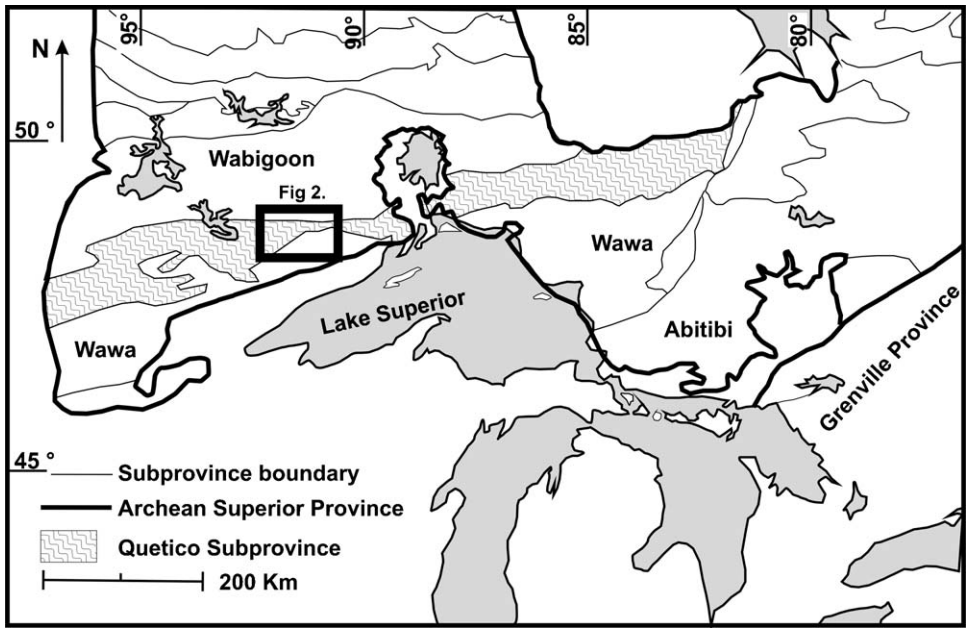

Fig. 1. Location map of the Quetico subprovince.

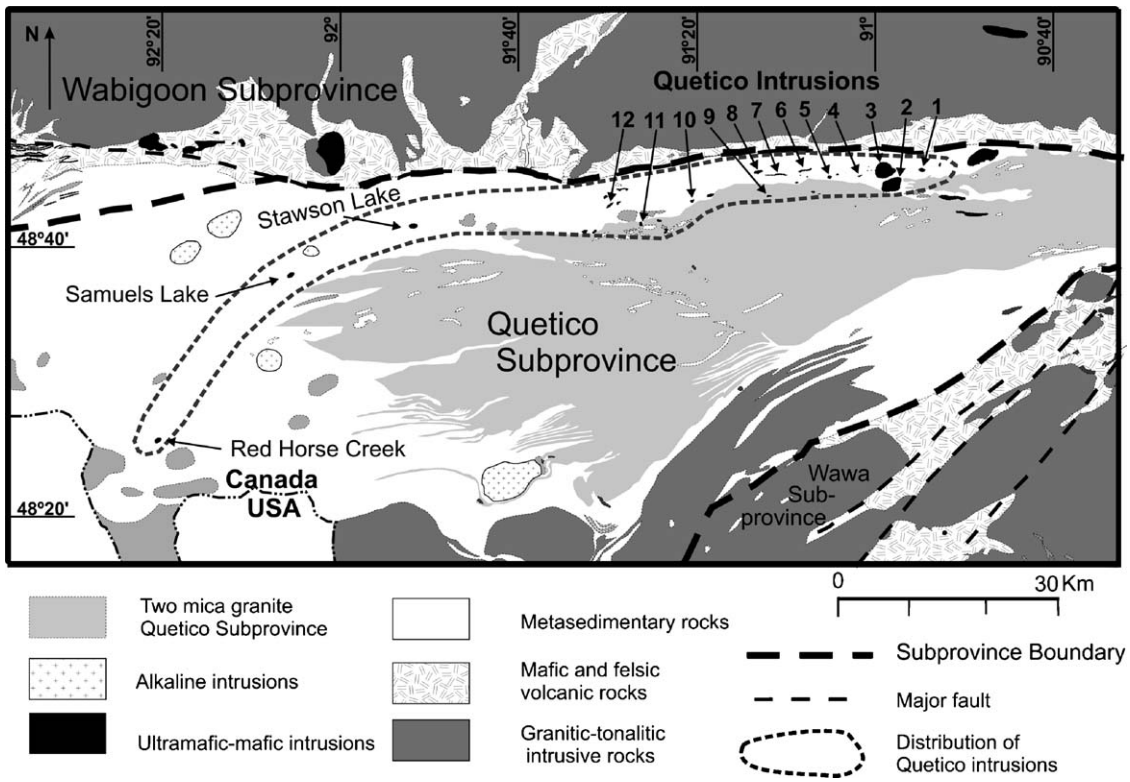

Fig. 2. Location map of the Quetico Intrusions. Several intrusions are less than 0.5 km in size and not appear on the map; relatively large classical Quetico Intrusions include: (1) Chief Peter, (2) South Elbow, (3) North Elbow, (4) Mud Lake, (5) Abiwin, (6) Heward Lake, (7) East Kawene, (8) Kawene Lake, (9) Eva Lake, (10) Nickelbe, (11) Nym Lake, (12) Plateau Lake. The distribution of the Quetico Intrusions is outlined with the thick dashed line.

derived magmas before cratonization of the Canadian Shield. These intrusions vary in size from 3 to 5 m thick dykes to elliptical stocks up to 3300 m × 1800 m in surface outcrop, and are zoned in lithology.

Apart from the array of mafic–ultramafic intrusions along the northern subprovince boundary, there are several mafic–ultramafic intrusions in the centre of the Quetico subprovince; not all intrusions are well described due to poor exposures and difficult access. We examined the intrusions in the centre of the Quetico subprovince and compared them with the intrusions along the northern boundary of the subprovince. Among them, we selected Samuels Lake intrusion for a detailed study due to availability of extensive drill core, and the lack of intense deformation of the intrusion. Our study includes detailed mapping of the intrusion, drill core logging, and a petrographic and bulk rock and mineral chemistry study of over 50 representative samples. For comparison, an additional 32 representative samples were examined from 10 other Quetico Intrusions, including those in the southern and northern portions of the subprovince. This paper documents the lithology, geochemistry, mineral chemistry, and the mineralization of a suite of mafic–ultramafic intrusions in the Quetico metasedimentary belt, discusses their origin, and compares them with mafic–ultramafic intrusions in Phanerozoic orogenic belts, and proposes a tectonic setting for the Archean mafic igneous rocks.

2. Regional geology

2.1. The Quetico subprovince

The Quetico subprovince is a linear metasedimentary belt bounded by two granite-greenstone belts, the Wabigoon subprovince to the north and the Wawa subprovince to the south (Fig. 1). The Quetico belt consists predominantly of metamorphosed greywackes and siltstones considered to have deposited in an accretionary prism that developed south of the Wabigoon arc before the collision of the Wawa arc from the south (e.g., Williams, 1991; Valli et al., 2004).

Four deformation events are recognized in the area. D1 included soft sediment deformation, minor isoclinal folding, and development of a planar fabric parallel to the original bedding (S1) shortly after sedimentation (Williams, 1991; Valli et al., 2004). D2 was mainly dextral strike slip shearing accompanied by folding and development of regional axial planar fabrics (S2). D3 was also transpressive, and produced upright, open to tight folding. This transpressive deformation most likely occurred during the oblique accretion of the Wawa belt to the Wabigoon subprovince to the north (Williams, 1991; Valli et al., 2004). The subsequent D4 was local, forming minor shear zones cutting fabrics developed earlier.

The Quetico subprovince contains five suites of plutonic rocks (Williams, 1991); (1) early mafic–ultramafic intrusions (i.e., Quetico Intrusions), (2) foliated tonalite and diorite with an age of ∼2688–2687 Ma (Davis et al., 1990), (3) syenitic rocks intruded at 2680 ± 1 Ma (Hattori and Percival, 1999), and (4) voluminous, peraluminous granitic rocks with an age of ∼2670–2653 Ma (Percival and Sullivan, 1988).

2.2. Quetico Intrusions

The term Quetico Intrusions was first used by Watkinson and Irvine (1964) to describe a group of small, mafic–ultramafic intrusions along the northern boundary of the Quetico subprovince (Fig. 2). They include the Chief Peter, Plateau Lake, Nym Lake, Eva Lake, North Elbow Lake, Mud Lake, Abiwin, Shepherd, and Kawene Lake intrusions (Fig. 2). The intrusions are mostly small (less than 3 km in diameter) and elongate in an E–W direction, except for the rounded North Elbow intrusion. Some, such as the Abiwin and Mud Lake intrusions, are narrow, less than 200 m N–S. Large intrusions commonly display lithological zoning from ultramafic cores to gabbroic rims. A detailed description of these northern intrusions appears in MacTavish (1999).

The Quetico Intrusions differ from older (ca. 2.73 Ga; Davis et al., 1989) mafic–ultramafic intrusions in the Wabigoon and Wawa greenstone belts (Fig. 2), such as the Bad Vermilion Lake, Grassy Portage, and Shebandowan complexes. These latter intrusions in greenstone belts are contemporaneous with volcanic rocks, are associated with komatiites and anorthosites, and may show varying lithological units, but there is no apparent zoning and no apparent alignments with regional fabrics (e.g., Poulsen and Hodgson, 1984; Blackburn et al., 1991).

Both alkaline and mafic–ultramafic intrusions in the Quetico subprovince exhibit strong positive aeromagnetic anomalies (Geological Survey of Canada and Ontario Department of Mines, 1965a,b) because metasedimentary host rocks and late granitic intrusions have low magnetic susceptibilities. After visiting these areas with aeromagnetic highs and examining rock samples, we identified three additional mafic–ultramafic intrusions in the center and southern part of the Quetico belt that are strikingly similar to those along the northern boundary. They are the Stawson Lake, Samuels Lake, and Red Horse Creek intrusions (Fig. 2). All three intrusions are relatively small (less than 1 km in diameter) and

have similar mineralogy and mineral chemistry, textures, lithology, and bulk rock compositions (see below). These findings increase the array of known Quetico Intrusions to over 125 km in length across the subprovince (Fig. 2).

3. Sampling and analytical method

Mapping, drill core logging, and sample collection were carried out in the summer of 1999 and 2000. Major and minor elements were determined on fused disks with Li borate using a Philips PW 2400 X-ray fluorescence spectrometer. Loss of ignition was determined after heating samples at 1050 °C for over 1.5 h. Sulphur and CO_2 contents were determined using a Leco elemental analyzer. The concentrations of rare earth elements (REE) and other trace elements were determined at using an inductively coupled plasma mass spectrometer (ICP-MS) after digesting samples with HNO_3–$HClO_4$–HF–HCl. The concentrations of PGEs for selected samples were determined by isotopic dilution technique using a mixed spike enriched in ^{99}Ru, ^{105}Pd, ^{190}Os, ^{191}Ir, and ^{194}Pt. The PGE with the spike solution and borate flux were pre-concentrated into a Ni bead. PGEs were then recovered from the bead by dissolving it in HCl solution. Insoluble PGE in HCl were recovered and dissolved in concentrated HNO_3 before the analysis of isotopic ratios with HP 4500 inductively coupled plasma mass spectrometer. The analytical procedure is essentially identical to that described in Guillot et al. (2000).

A total of 87 grains of olivine, clinopyroxene, amphibole, and mica were analyzed from nine representative samples from the Samuels Lake intrusion (Fig. 3). Mineral compositions were determined using a Camebax MBX electron microprobe by wavelength dispersive X-ray analysis. Operating conditions were 15 kV accelerating voltage and 20 nA specimen current. Counting time was 15–40 s or 40,000 accumulated counts for each

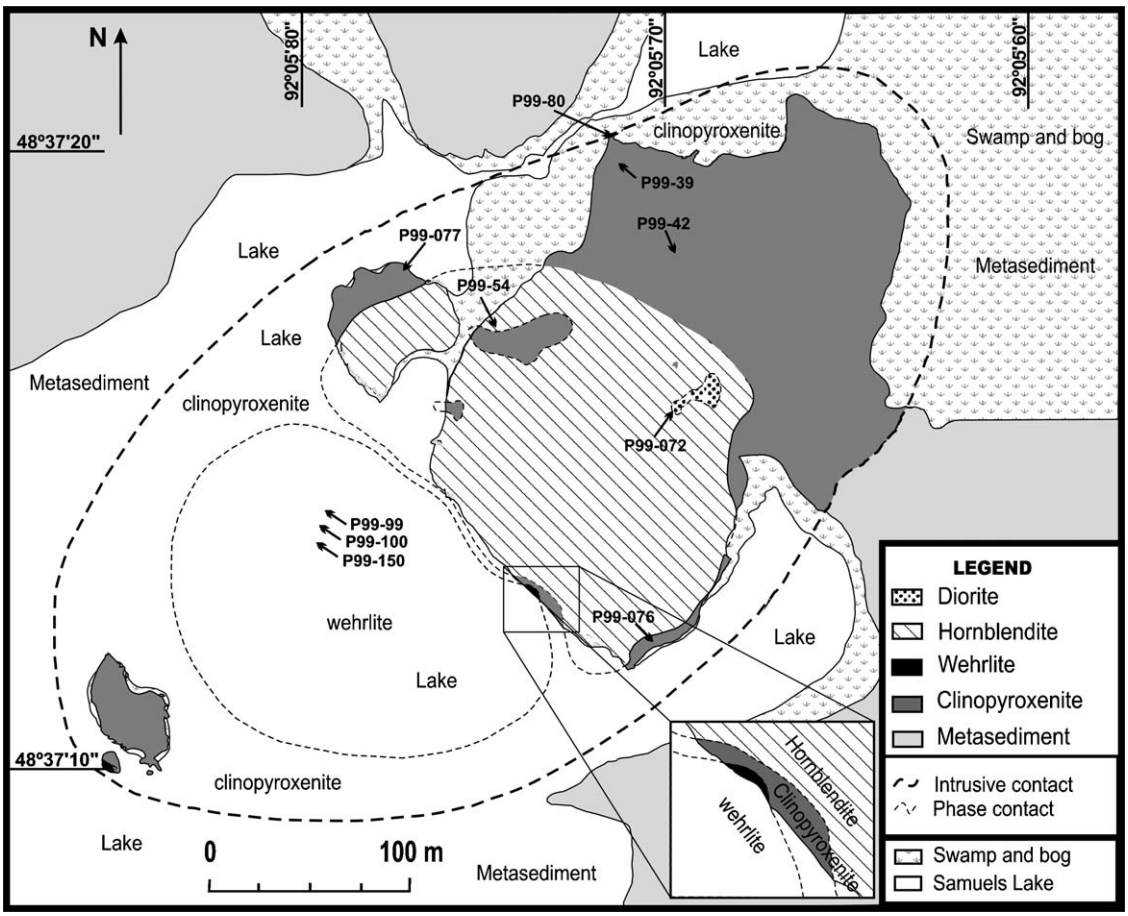

Fig. 3. Geological map of the Samuels Lake intrusion, modified after Pettigrew et al. (2000). The locations of samples used for mineralogical and bulk rock analysis in Tables are shown with arrows. The tips of the arrows correspond to the locations. Note that samples from drill core are beneath Samuels Lake and shown in the lake in the diagram.

element. A suite of well characterized natural and synthetic minerals and compounds were used as calibration standards for silicate analysis. The raw X-ray data were converted to weight% by the Cameca PAP matrix correction program. Analyses were accurate to ±1–2% for major elements, and ±3–5% for minor elements (i.e., <1 wt.%).

4. Samuels Lake intrusion

The Samuels Lake intrusion has a NE–SW elliptical (500 m × 250 m) shape, which is parallel to the regional fabrics, and the contacts with sedimentary rocks are steeply dipping and sharp. The interior shows very little deformation, mostly in the form of narrow, conjugate brittle–ductile shears and local, poorly developed fractures.

The intrusion shows weak concentric zoning with a wehrite core grading into clinopyroxenite toward the rim (Fig. 3). These units were subsequently intruded by hornblendite, and finally by small diorite dikes and plugs (Fig. 3). The diorite unit contains angular fragments and breccias of wehrite and clinopyroxenite (Fig. 4E and F), indicating its intrusion after the solidification of these earlier phases. Zircon grains in the diorite phase yielded a U–Pb age of 2688 + 6/−5 Ma (McNicoll, Pettigrew, unpublished data, 2000), which provides the minimum age of the intrusion.

The intrusion has undergone several phases of alteration and metamorphism: intrusion-related alteration, low amphibolite-facies regional metamorphism, and late retrograde alteration. It is not easy to differentiate the first two, but we consider that the serpentinization of olivine and hydration of clinopyroxene most likely took place during the intrusive activity, based on the distribution of the alteration minerals. The serpentinization of olivine is restricted to grains in contact with sulphides in wehrlite, whereas olivine in sulphide-poor clinopy-

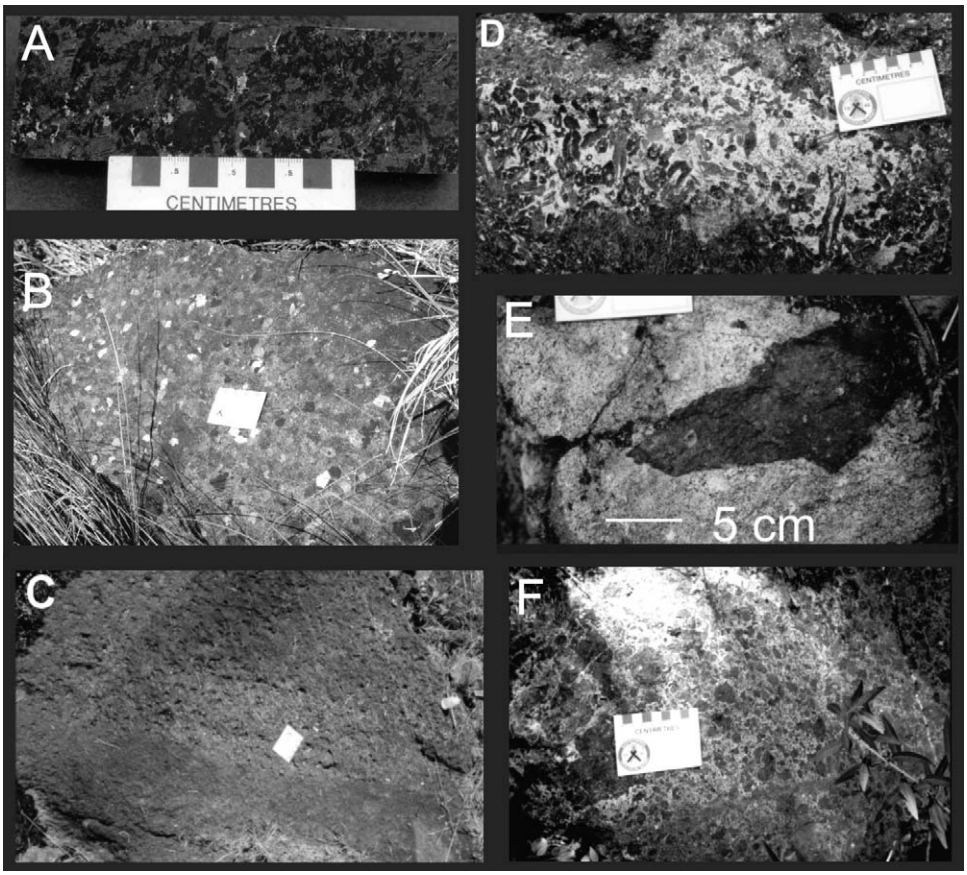

Fig. 4. Photographs of representative lithological units of the Samuels Lake intrusion: (A) werhlite containing serpentinized olivine (black) and minor disseminated Cu–Ni sulphides (lighter color), (B) clinopyroxenite showing the crystal faces of coarse diopsidic clinopyroxene, (C) weathered surface of hornblendite with abundant pits due to erosion of biotite, (D) pegmatite containing plagioclase-cored hornblende, (E) late diorite containing an angular fragment of clinopyroxenite and werhlite, (F) diorite (matrix) breccia with abundant fragments of clinopyroxenite and werhlite (dark).

roxenite shows little alteration. This evidence suggests that aqueous fluids released from sulphide melt were likely responsible for the hydration of olivine. Sulphide melt in hydrous magma may contain significant H_2O (Wykes and Mavrogenes, 2005), and the water released from solidifying sulphides results in the hydration of surrounding silicate minerals (e.g., Pettigrew and Hattori, 2002). Replacement of clinopyroxene by hornblende and a mixture of hornblende and actinolite in werhlite and clinopyroxenite may also have taken place during the intrusion.

The regional metamorphism of low amphibolite facies affected the intrusion and surrounding rocks. In sedimentary rocks, garnet and hornblende formed during this metamorphism. Inside the intrusion, such metamorphism caused the formation of tabular titanite in amphiboles. It is also possible that some clinopyroxene grains were replaced by hornblende during this regional metamorphism. Titanite grains along the cleavages of hornblende (Fig. 5A) gives the U–Pb age of this event, 2668 ± 6 Ma (McNicoll, Pettigrew, unpublished data, 2000). The age is consistent with the inferred age, ~2670 Ma, of the peak regional metamorphism of sedimentary rocks in the area (Valli et al., 2004).

Late retrograde metamorphism to greenschist facies resulted in minor chloritization of hornblende and mica, saussuritization of plagioclase, and minor quartz + carbonate veinlets along fractures in the intru-

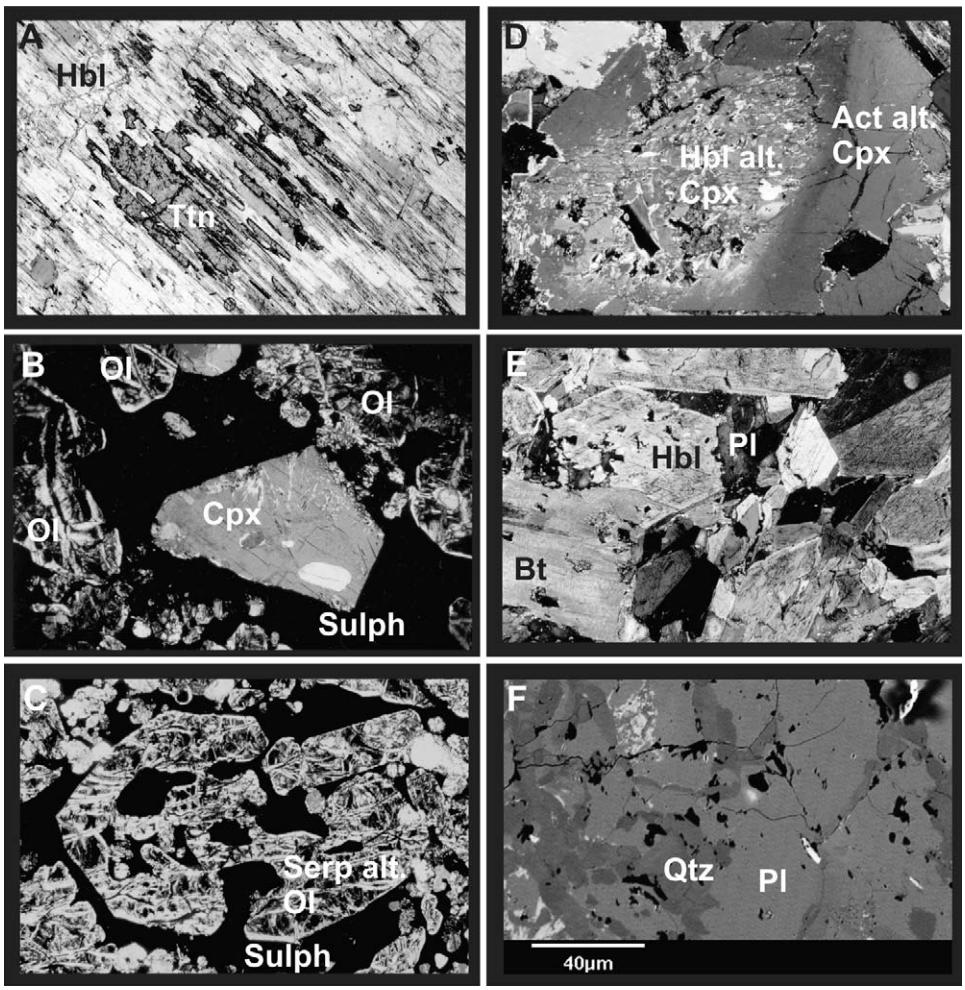

Fig. 5. Photomicrographs and back-scattered electron images of representative rocks of the Samuels Lake intrusion. (A) Secondary titanite (Ttn) in hornblende (Hbl) in pegmatite, (B) typical appearance of wehrite containing unaltered diopsidic clinopyroxene (Cpx) and serpentinized olivine (Ol) surrounded by sulphide minerals (Sulph). Sulphides minerals are mostly pyrrhotite with chalcopyrite and pentlandite, (C) serpentinized olivine (Serp alt. Ol) in sulphide matrix in wehrite, (D) clinopyroxenite where the core of diopside is altered to hornblende (Hbl alt. Cpx) and rim is altered to actinolite (Act alt. Cpx), (E) euhedral hornblende (Hbl) and phlogopitic biotite (Bt) in the hornblendite, (F) back-scattered electron image of diorite exhibiting myrmekitic intergrowth of quartz (Qtz) and plagioclase (Pl). Field of view in all photomicrographs is 2.5 mm.

sion. In sedimentary rocks, garnet and hornblende grains were partially altered to chlorite.

4.1. Petrology of various units of the Samuels Lake intrusion

4.1.1. Wehrite

The wehrite unit underlies Samuels Lake and its distribution shown in Fig. 3 is based primarily on diamond drill core data. The unit shows cumulus texture with euhedral to subhedral olivine and clinopyroxene (Mg#, atomic ratio of Mg/[Mg + Fe2+] of 0.85–0.95; Table 1b) in a matrix of sulphides and anhedral hornblende (Mg# ~0.94; Table 1c), magnetite (Figs. 4A and 5B and C) and minor phlogopite (Mg# 0.90–0.91; Table 1d). Olivine grains are pseudomorphed by serpentine (Fig. 5B and C), and the pseudomorphs contain unaltered clinopyroxene grains. Early crystallization of clinopyroxene and late crystallization of plagioclase imply elevated water contents in the parental magmas, as water widens the clinopyroxene liquidus field at the expense of plagioclase (e.g., Gaetani et al., 1993).

Sulphide contents are generally high, greater than 3 vol.% and up to 40 vol.% within this unit. Sulphides display blebby to net textures surrounding olivine and clinopyroxene grains. The occurrence of exsolved pentlandite and chalcopyrite in pyrrhotite indicates that the sulphides were once a monosulphide solid solution. Sulphide-rich rocks show extensive hydration, and contain serpentinized olivine and a mixture of secondary hornblende + amphibole ± chlorite as replacements of clinopyroxene and hornblende. These aggregates show globular grey patches in black serpentinized olivine, which gives the unit a distinct appearance (Fig. 4A).

The net-textured sulphide with olivine and the embayment of sulphides into olivine crystals (Fig. 5B and C) indicate the separation of an immiscible sulphide melt during the crystallization of olivine. This is consistent with low Ni contents (up to 0.1 wt.% NiO; Table 1a) of olivine in clinopyroxenite samples, because Ni is preferentially incorporated in sulphide melt. Nickel contents of olivine in wehrlite could not be determined because of extensive serpentinization.

Magnetite contents are high, up to 10 vol.%, in sulphide-rich phases. Magnetite occurs as fine dusty dissemination in serpentine and anhederal grains associated with sulphides. The former likely crystallized from Fe released during the transformation of olivine to serpentine. Magnetite associated with sulphides (up to 5 vol.%) likely formed during the solidification of sulphide melt as sulphide melt can dissolve significant concentrations of O (up to 14 wt.% O; Francis, 1990).

Table 1a
Composition of representative grains of olivine

	Sample (Unit[a])				
	P99-60 (Wehr)		P99-42 (Cpxt)		P99-118 (Cpxt)
Intrusions	Core of N.Elbow		Rim of Samuels		Rim of E. Kaw
SiO_2	37.7	37.6	40.0	39.5	38.7
FeO	22.3	22.1	20.2	20.7	18.5
MgO	38.9	38.7	39.1	39.0	42.2
MnO	0.30	0.40	0.47	0.47	0.30
NiO	0.10	0.10	0.09	0.08	0.20
Sum	99.3	98.9	99.93	99.76	99.9
Formula based of 4 oxygens					
Si	0.99	0.991	1.028	1.021	0.991
Fe^{2+}	0.49	0.487	0.434	0.447	0.396
Mg	1.522	1.520	1.498	1.50	1.611
Mn	0.007	0.009	0.01	0.01	0.007
Ni	0.002	0.002	0.002	0.002	0.004
Sum	2.021	2.018	1.944	1.959	2.019
Mg#	0.756	0.757	0.775	0.770	0.803

Compositions of representative minerals from the Quetico Intrusions. *Intrusions*: P99-60, Lake intrusion, at 645863E, 5402925N; P99-42, Lake, drill hole P5-2; P99-118, Lake, 632407E, 5402297N. All UTM coordinates are in NAD 27 Zone 15. Note that olivine grains in wehrlite in the Samuels Lake intrusion are all serpentinized.

[a] Cpxt, clinopyroxenite; Wehr, wehrite.

4.1.2. Clinopyroxenite

Clinopyroxenite is the most voluminous unit of the intrusion and is well exposed on surface (Fig. 3). This unit displays cumulate textures and is comprised of coarse-grained (commonly greater than 2 cm) clinopyroxene (Mg# 0.84–0.91; Table 1b) with minor interstitial calcic amphibole (Mg# 0.73–1.00; Table 1c), phlogopite (Mg# ~0.90; Table 1d), magnetite, ± olivine (Mg# 0.77–0.78; Table 1a) ±plagioclase. The unit commonly displays poikilitic textured amphibole or clinopyroxene enclosing fine to medium-grained clinopyroxene (Figs. 4B and 5D), and grades into plagioclase-bearing clinopyroxenite, or melanocratic gabbro near the contacts with sedimentary country rocks.

Clinopyroxene is predominantly diopside (Fig. 8; Table 1b) and plots in the sub-alkaline field, as defined by Le Bas (1962) (Fig. 9). Amphiboles are calcic and mostly secondary replacement products of clinoproxene, but amphibole grains interstitial to clinopyroxene in less altered samples may be primary. Amphibole shows a compositional variation even in one sample, ranging from magnesiohornblende to magnesiohastingsite to edenite, following the classification of Leake et al. (1997). The wide compositional variation is attributed to the effect of hydrothermal alteration probably during the intrusive activity.

Sulphide contents are generally low in clinopyroxenite, less than 0.1 vol.%, with locally high, up to 3 vol.%, Cu-rich sulphides. The sulfide abundance is independent of olivine content. Pyrrhotite is the major mineral with minor chalcopyrite and pentlandite. Magnetite contents are minor in quantity (up to 5%) and it occurs interstitial to silicate minerals and locally as intergrowths with clinopyroxene.

4.1.3. Hornblendite

Hornblendite intruded semi-solidified wehrite and clinopyroxenite, producing a texture of magma mingling

Table 1b
Composition of representative grains of clinopyroxene

	Sample (Unit[a])				
	P99-99 (Wehr)	P99-100 (Wehr)	P99-60 (Wehr)	P99-118 (Wehr)	P99-39 (Cpxt)
SiO_2	52.9	52.7	52.3	52.7	53.4
Al_2O_3	1.95	1.8	1.8	1.7	1.9
Fe_2O_3	1.63	2.71	0.96	1.41	1.75
TiO_2	<0.05	0.2	0.1	0.2	0.17
Cr_2O_3	0.68	0.5	0.2	0.9	0.3
MgO	17.3	18.0	17.2	17.3	17.6
FeO	2.79	1.67	5.83	2.03	3.03
MnO	0.2	0.2	0.3	0.2	0.11
CaO	22.2	21.0	19.5	22.4	22.2
Na_2O	0.24	0.5	0.2	0.3	0.25
Sum	99.91	99.28	98.39	99.14	100.71
Formula based of 6 oxygens					
Si	1.934	1.929	1.948	1.936	1.935
Al	0.066	0.071	0.052	0.064	0.065
ΣT	2.00	2.00	2.00	2.00	2.00
Al	0.018	0.007	0.027	0.01	0.016
Fe^{+3}	0.045	0.075	0.027	0.039	0.048
Ti	0	0.006	0.003	0.006	0.005
Cr	0.02	0.014	0.006	0.026	0.009
Mg	0.942	0.982	0.955	0.947	0.948
Fe^{+2}	0.085	0.051	0.182	0.063	0.092
Mn	0.006	0.006	0.009	0.006	0.003
Ca	0.869	0.824	0.778	0.882	0.861
Na	0.017	0.035	0.014	0.021	0.018
ΣAB	2.00	2.00	2.00	2.00	2.00
Mg #	0.917	0.951	0.840	0.938	0.912

Intrusions: P99-60, P99-118, see Table 1a. Samples P99-99 and P99-100 from Samuels Lake intrusion are from drill core DDH 3 at depth of 204.3 m and 212.8 m, respectively. The location of P99-39 is shown on Fig. 3.

[a] Cpxt, clinopyroxenite; Wehr, wehrite.

Table 1c
Composition of representative grains of amphiboles

	Sample (Unit[a])										
	P99-99 (Wehr)	P99-60 (Wehr)		P99-39 (Cpxt)		P99-76 (Cpxt)	P99-77 (Peg)	P99-54 (Hbldt)		P99-72 (Dior)	
SiO_2	43.7	41.9	45.3	47.0	49.6	43.2	49.2	43.2	47.0	49.5	45.2
Al_2O_3	10.6	12.5	9.7	8.67	6.75	12.00	6.33	13.5	10.7	6.21	9.99
TiO_2	0.28	1.8	0.6	0.4	0.4	0.5	0.24	1.14	0.59	0.18	0.44
Cr_2O_3	0	0.3	0.4	1.15	1.04	<0.04	<0.04	<0.04	<0.04	0.05	0.04
Fe_2O_3	3.85	8.14	8.64	3.86	4.32	6.76	4.04	3.78	3.13	6.92	5.68
FeO	2.75	1.68	1.22	3.98	2.92	5.1	6.69	8.11	8.02	8.51	11.6
MnO	0	0.1	0.1	0.18	0.11	<0.04	0.2	0.14	0.16	0.35	0.27
MgO	17.8	15.5	16.7	17.7	19.1	14.6	16.0	13.2	14.5	14.0	11.3
CaO	12.4	10.9	11.4	12.5	12.7	11.8	12.2	11.8	12.0	11.6	11.6
Na_2O	2.52	2.3	1.7	2.45	1.97	2.07	1.03	2.04	2.06	1.22	1.9
K_2O	0.87	1.1	0.8	0.15	0.08	0.76	0.25	1.17	0.22	0.15	0.39
F	0	0.40	0.1	0.1	<0.05	<0.05	0.08	0.08	0.16	0.06	0.11
Sum	94.69	96.62	96.66	98.21	98.96	96.7	96.21	98.21	98.6	98.71	98.47
Formula based on 23 oxygens											
Si	6.44	6.13	6.54	6.70	6.94	6.33	7.15	6.28	6.72	7.12	6.64
Al	1.56	1.88	1.46	1.31	1.06	1.67	0.849	1.72	1.28	0.884	1.36
ΣT	8.00	8.00	8.00	8.00	8.00	8.00	8.00	8.00	8.00	8.00	8.00
Al	0.279	0.278	0.193	0.151	0.054	0.398	0.234	0.597	0.524	0.168	0.372
Ti	0.031	0.198	0.065	0.043	0.042	0.055	0.026	0.125	0.063	0.019	0.049
Cr	0	0.035	0.046	0.13	0.115	0	0.001	0	0	0.006	0.005
Fe^{+3}	0.428	0.895	0.939	0.414	0.455	0.745	0.442	0.414	0.337	0.748	0.628
Fe^{+2}	0.339	0.205	0.148	0.474	0.342	0.625	0.813	0.986	0.959	1.023	1.427
Mn	0	0.012	0.012	0.022	0.013	0	0.024	0.017	0.019	0.043	0.034
Mg	3.92	3.38	3.60	3.77	3.98	3.18	3.46	2.861	3.097	2.994	2.486
ΣA	5.00	5.00	4.998	5.000	4.999	4.999	5.000	5.000	4.999	5.001	5.001
Ca	1.952	1.707	1.764	1.912	1.901	1.844	1.892	1.835	1.843	1.778	1.822
Na	0.048	0.293	0.236	0.088	0.099	0.156	0.108	0.165	0.157	0.222	0.178
ΣB	2	2.00	2.00	2.00	2.00	2.00	2.00	2.00	2.00	2.00	2.00
Na	0.672	0.359	0.24	0.589	0.436	0.432	0.181	0.41	0.414	0.118	0.364
K	0.163	0.205	0.147	0.027	0.014	0.141	0.047	0.217	0.04	0.027	0.073
ΣA	0.835	0.564	0.387	0.616	0.45	0.573	0.228	0.627	0.454	0.145	0.437
F	0	0.185	0.046	0.045	0	0	0.034	0.037	0.072	0.027	0.051
Mg#	0.94	0.94	0.96	0.89	0.92	0.84	0.81	0.74	0.76	0.75	0.64
Name[b]	Mg-Hst	Mg-Hst	Mg-Hst	Edn	Mg-Hbl	Mg-Hst	Mg-Hbl	Prg	Mg-Hbl	Mg-Hbl	Mg-Hbl

Chlorine contents were below the detection limit of 0.1 wt.%. *Intrusions:* P99-60, see Table 1a. Locations of samples (P99-99, P99-39P99-76, P99-77, P99-54, P99-72) from Samuels Lake intrusions are shown on Fig. 3.

[b] Classification following Leak et al. (1997). Edn: edenite, Mg-Hst: Magnesiohastingsite, Mg-Hbl: magnesiohornblende, Prg: pargasite.

[a] Cpxt, clinopyroxenite; Dior, quartz diorite; Hbldt, hornblendite; Wehr, wehrite, Peg, pegmatite.

and local brecciation. This unit itself formed by multiple pulses of intrusions based on the occurrence of the fragments of earlier hornblendite with different grain sizes and plagioclase contents. Some pulses intruded as a crystal mush, based on alignment of hornblende crystals parallel to the contacts. This unit is medium grained and composed almost entirely of subhedral, elongate crystals of pargasitic to magnesio hornblende (Mg# 0.72–0.76; Table 1c) with interstitial plagioclase, phlogopite (Mg# ~0.72; Table 1d), titanite, and trace K-feldspar, ilmenite, pyrrhotite, and pyrite (Figs. 4C and 5E). The essentially monomineralic nature of the unit along with its subhedral hornblende crystals and fine-grained matrix of plagioclase + phlogopite indicate that this unit is also of cumulate origin.

4.1.4. Pegmatite

Pegnatite forms dykes and pods and occurs in all rock types. The unit is composed of large (2–10 cm) euhedral to subhedral crystals of hornblende (Mg# ~0.81; Table 1c) containing plagioclase cores within a plagioclase matrix (Fig. 4D), and also contains significant

Table 1d
Composition of representative grains of biotite and phlogopite

	Sample (Unit[a])					
	P99-99 (Wehr)		P99-118 (Cpxt)	P99-54 (Hbldt)	P99-72 (Dior)	P99-77 (Peg)
SiO_2	41.0	39.2	39.0	37.6	36.50	35.8
Al_2O_3	13.4	13.8	14.8	15.8	15.3	15.8
TiO_2	0.34	0.38	0.6	1.52	2.8	1.98
Cr_2O_3	0.26	0.3	0.4	<0.05	<0.05	<0.05
Fe_2O_3	4.29	4.51	5	12.17	19	14.98
MnO	<0.05	<0.05	<0.05	0.14	0.16	0.12
MgO	24.3	23.9	24.2	17.1	12.1	14.9
Na_2O	0.42	0.39	0.3	0.43	0.1	0.19
K_2O	9.06	9.31	9.1	9.17	9.34	8.9
Sum	93.13	91.73	93.4	93.98	95.3	92.63
Formula based on 22 oxygens						
Si	5.92	5.77	5.65	5.61	5.56	5.50
Al	2.084	2.231	2.351	2.393	2.44	2.50
ΣT	8.00	8.00	8.000	8.00	8.00	8.00
Al	0.195	0.164	0.175	0.384	0.302	0.356
Ti	0.037	0.042	0.065	0.17	0.321	0.228
Cr	0.03	0.035	0.046	0	0	0.006
Fe	0.517	0.556	0.606	1.518	2.421	1.924
Mn	0	0	0.000	0.018	0.021	0.015
Mg	5.222	5.246	5.225	3.809	2.757	3.411
ΣM	6.001	6.043	6.117	5.9	5.822	5.940
Na	0.117	0.112	0.084	0.124	0.03	0.058
K	1.665	1.749	1.681	1.744	1.816	1.745
ΣI	1.782	1.861	1.765	1.868	1.846	1.803
Mg#	0.910	0.904	0.896	0.715	0.532	0.639
	Phl	Phl	Phl	Bt	Bt	Bt

P99-118, see Table 1a; P99-54, P99-72, P99-77, P99-99, all on Fig. 3.
[a] Cpxt, clinopyroxenite; Dior, quartz diorite; Hbldt, hornblendite; Peg, pegmatite; Wehr, wehrlite; Bt, biotite; Phl, phlogopite.

Table 1e
Composition of representative grains of apatite in Samuels Lake intrusion

	Sample (Unit[a])				
	P99-039 (Cpxt)	P99-054 (Hbldt)	P99-080 (Gabb)	P99-072 (Dior)	P99-077 (Peg)
CaO	52.5	54	54.1	54.7	54.4
FeO	0.1	0.1	0.06	0.10	0.07
MnO	0.1	0.1	<0.05	0.10	<0.05
P_2O_5	41.8	41.8	41.9	41.2	41.3
F	1.8	3.1	3.1	2.6	3.2
Cl	0.6	<0.1	<0.1	<0.1	<0.1
Sum	96.9	99.1	99.18	98.7	98.93
Formula based on 25 oxygens					
Ca	9.486	9.554	9.559	9.762	9.667
Fe^{2+}	0.014	0.014	0.008	0.014	0.010
Mn	0.014	0.014	0	0.014	0
P	5.968	5.844	5.849	5.810	5.795
F	0.960	1.619	1.622	1.370	1.658
Cl	0.171	0	0	0	0

The contents of SrO, MgO and SiO_2 were below 0.04 wt.%. Sample locations are shown in Fig. 3.
[a] Cpxt, clinopyroxenite; Gabb, gabbro; Hbldt, hornblendite; Peg, pegmatite.

Table 2
Representative bulk rock compositions of Quetico Intrusions

	Sample (Unit[a])												
	P99 150 (Wehr)	P99-177 (Wehr)	P99-076 (Cpxt)	P99-059a (Cpxt)	P99-116 (Cpxt)	P99-028 (Cpxt)	P99-114 (Cpxt)	P99-175 (Cpxt)	P99-54 (Hbldt)	P99-059b (Hbldt)	P99-027 (Hbldt)	P99-174 (Gabb)	P99-072 (Dior)
SiO_2	38.9	43.7	47.3	47.1	48.4	47.4	47.4	46.7	45.0	48.8	44.7	52.1	57.6
TiO_2	0.12	0.30	0.35	0.85	0.90	0.58	0.25	0.65	1.45	0.67	1.30	0.76	0.53
Al_2O_3	2.6	5.30	5.1	8.8	8.80	7.50	3.7	8.70	13.9	15.7	11.4	15.3	20.5
Fe_2O_3	nd.	nd.	3	3.8	nd.	nd.	4.9	nd	2.90	2.80	nd	2.6	0.80
FeO	ϕ 16.7	ϕ 10.5	6.6	8.2	ϕ 11.0	ϕ 10.9	4.5	ϕ 10.0	8.5	6.8	ϕ 11.3	6.1	3.0
MnO	0.15	0.18	0.14	0.2	0.18	0.19	0.15	0.15	0.12	0.16	0.15	0.16	0.04
MgO	29.0	24.43	17.77	14.2	13.330.18	15.2	22.3	16.2	12.1	9.56	13.3	7.19	2.23
CaO	3.21	7.95	14.0	12.1	12.83	12.9	12.3	11.5	10.11	8.65	12.3	7.35	5.13
Na_2O	0.1	0.70	0.8	1.4	1.7	1.00	0.5	1.10	2.5	3.1	1.5	4.1	6.5
K_2O	0.24	0.46	0.21	0.65	0.70	0.73	0.31	0.89	1.67	1.4	1.0	1.61	2.08
$H_2O(+)$	nd	6.1	2.4	2.3	2.3	2.7	3.7	2.9	1.8	1.6	2.5	2	1.3
CO_2	0.2	0.5	2.4	0.6	0.5	1.4	0.9	0.5	0.2	0.2	0.7	0.6	0.2
P_2O_5	0.06	0.07	0.07	0.24	0.08	0.10	0.05	0.03	0.09	0.39	0.07	0.43	0.43
S	1.9	0.02	0.6	0.46	0.03	0.11	0.12	0.12	0.34	0.43	0.11	0.08	0.17
LOI	5.3												
sum	98.4	100.2	100.7	100.9	100.7	100.7	101.1	99.5	100.7	100.3	100.3	100.4	100.5
Ba (ppm)	79	140	57	190	290	220	90	150	350	370	270	460	720
Co (ppm)	270	103	92	68	63	80	77	87	71	58	74	37	12
Cr (ppm)	320	2100	1100	860	800	480	2100	1400	247	381	344	303	36
Cs (ppm)	0.9	0.79	0.18	0.31	1.50	25	7.7	1.60	1.3	1.8	15	1.8	1.4
Cu (ppm)	1750	628	2880	183	43	113	57	2550	150	170	160	52	85
Hf (ppm)	0.53	0.99	0.77	2.1	2.20	1.0	0.55	1.2	1.7	1.3	1.3	1.7	4.7
Nb (ppm)	0.97	1.70	0.99	4.3	7.10	1.7	0.93	1.9	3.3	2.8	2.3	4.4	5.2
Ni (ppm)	1460	674	579	196	144	130	350	464	92	124	93	85	11
Rb (ppm)	8.1	3.60	1.7	12	13	19	9.1	18	29	44	20	66	45
Sc (ppm)	11	25	46	54	52	52	34	45	61	36	75	21	4
Sr (ppm)	73	110	130	220	360	230	190	79	430	740	340	980	1600
Ta (ppm)	0.06	0.11	0.06	0.23	0.32	0.11	0.05	0.12	0.17	0.15	0.15	0.16	0.3
Th (ppm)	0.85	0.62	0.73	1.4	3.10	0.86	0.52	0.8	1.2	0.77	0.75	1.1	16
U (ppm)	0.29	0.78	0.2	0.41	1.0	0.29	0.15	0.64	0.4	0.25	0.19	0.31	1.7
V (ppm)	39	146	160	260	260	230	105	247	430	200	430	170	97
Zn (ppm)	105	80	53	86	85	83	41	68	56	77	75	88	29
Zr (ppm)	24	32	27	66	70	34	21	38	52	44	36	74	240
Y (ppm)	3	9.2	7.4	21	18	12	5.7	13	20	15	18	16	6
La (ppm)	5.3	5.7	13	16	15	6.7	5.6	5.0	11	16	6.9	37	100
Ce (ppm)	11	14	25	46	38	18	13	15	32	39	21	82	175
Pr (ppm)	1.3	1.9	3.1	6.5	5.5	2.8	1.9	2.3	4.9	5	3.4	10	17
Nd (ppm)	5.5	7.8	13	29	25	13	8.3	11	25	22	17	43	52
Sm (ppm)	0.98	1.8	2.7	6.1	5.8	2.9	1.7	2.3	5.7	4.7	4.3	7	5.8
Eu (ppm)	0.27	0.59	0.67	1.6	1.5	0.84	0.52	0.66	1.6	1.3	1.3	1.8	1.4
Gd (ppm)	0.7	1.8	2.1	5.6	5.3	2.8	1.5	2.5	5.2	4.1	4.3	4.7	2.8

Table 2 (*Continued*)

	Sample (Unit[a])												
	P99 150 (Wehr)	P99-177 (Wehr)	P99-076 (Cpxt)	P99-059a (Cpxt)	P99-116 (Cpxt)	P99-028 (Cpxt)	P99-114 (Cpxt)	P99-175 (Cpxt)	P99-54 (Hbldt)	P99-059b (Hbldt)	P99-027 (Hbldt)	P99-174 (Gabb)	P99-072 (Dior)
Dy (ppm)	0.51	1.5	1.5	4	3.5	2.2	1.1	2.2	3.8	2.9	3.4	3	1.2
Ho (ppm)	0.09	0.32	0.26	0.78	0.65	0.46	0.19	0.46	0.69	0.55	0.68	0.52	0.2
Er (ppm)	0.25	0.92	0.65	2	1.7	1.2	0.47	1.3	1.7	1.4	1.8	1.3	0.49
Yb (ppm)	0.25	0.83	0.64	1.9	1.4	1.2	0.47	1.1	1.5	1.3	1.5	1.3	0.51
Lu (ppm)	0.04	0.13	0.09	0.28	0.20	0.16	0.07	0.17	0.21	0.19	0.22	0.21	0.1
Pt (ppb)	17	nd	1500	nd	nd	nd	nd	nd	3.17	nd	0.64	nd	0.02
Pd (ppb)	14	nd	1270	nd	nd	nd	nd	nd	3.76	nd	0.99	nd	0.56
Ru (ppb)	0.38	nd	3.0	nd	nd	nd	nd	nd	0.06	nd	nd	nd	0.07
Os (ppb)	0.73	nd	2.7	nd	nd	nd	nd	nd	0.12	nd	nd	nd	0.14
Ir (ppb)	0.50	nd	19	nd	nd	nd	nd	nd	0.06	nd	nd	nd	0.02
Re (ppb)	5.1	nd	0.33	nd	nd	nd	nd	nd	0.33	nd	nd	nd	0.20

The locations of samples from Samuels Lake intrusion (Sam) are shown in Fig. 3. P99-059a, rim of the North Elbow Lake intrusion (N. Elb) at 647768E, 5402531N; P99-116, rim of Kawene Lake intrusion at 630123E, 5402099N; P99-028, rim of Mud Lake intrusion (Mud) at 643850E, 5402400N; P99-114, rim of Kawene Lake intrusion (Kaw); P99-175, rim of Red Horse Creek intrusion (Red) at 548420E, 5362090N; P99-059b, North Elbow (N. Elb), 647768E, 5402531N; P99-27, Mud Lake (Mud) at 643775E, 5402390N; P99-174, South Elbow Lake intrusion (S. Elb) at 647675E, 5400961N; all UTM coordinates are in NAD 27 Zone 15. Φ, Total Fe expressed as FeO, nd, not determined.

[a] Cpxt, clinopyroxenite; Dior, diorite; Gabb, gabbro; Hbldt, hornblendite.

amounts of biotite (Mg# ∼0.64; Table 1d), K-feldspar, titanite, zircon, and apatite (Table 1e). Minor quartz and carbonate occur in some pegmatite veins. Zircon grains are common, but none are suitable for U–Pb age determination because of a high degree of radiation damage.

4.1.5. Diorite

Diorite is the youngest unit, forming dykes and plugs with abundant angular fragments of wehrite and clinopyroxenite (Fig. 4F), and is volumetrically minor in comparison to other units; it commonly intruded along the contact with the metasedimentary host rocks. This unit locally grades into hornblende gabbro, quartz-diorite, monzodiorite, and quartz monzodiorite. This unit is medium grained (∼2 mm) and composed primarily of plagioclase, magnesiohornblende (Mg# 0.63–0.75; Table 1c), quartz, microcline, and biotite (Mg# ∼0.53; Table 1d), with trace ilmenite, pyrrhotite, F-rich apatite (Table 1e), titanite, monazite, and zircon, and displays well-developed myrmekitic textures (Fig. 5F). The parental magmas were volatile-rich, forming breccias with abundant fragments of clinopyroxenite (Fig. 4F). Alteration forming K-feldspar and epidote developed immediately adjacent to the diorite dykes, probably due to the release of aqueous fluid during solidification of the unit.

4.1.6. Cu–Ni–PGE mineralization

Cu–Ni–PGE mineralization occurs mostly in sulphide-rich portions of wehrite unit. The sulphides consist of pyrrhotite, chalcopyrite, and pentlandite with up to 2.63 wt.% Cu, up to 0.68 wt.% Ni, up to 940 ppb Pt, 900 ppb Pd, and 330 ppb Au. Most wehrite, however, contains moderate concentrations, ∼0.50 wt.% Cu, ∼0.45 wt.% Ni, and ∼0.04 wt.% Co, ∼180 ppb Pt, ∼230 ppb Pd, and ∼100 ppb Au (Pettigrew et al., 2000). The clinopyroxenite unit contains low sulphides, less than 1 vol.%, with low Cu and Ni, but there are sporadic occurrences of sulphides in veins recording up to 1500 ppb Pt, 1270 ppb Pd, and 0.29 wt.% Cu (Table 2).

4.2. Geochemistry of the Samuels Lake intrusion

4.2.1. Effects of intrusion-related alteration

The Samuels Lake intrusion has undergone intrusion-related alteration and regional lower amphibolite-facies metamorphism. This history limits the use of fluid-soluble elements for petrogenetic study, but high field strength elements (HFSE) are generally considered immobile during intrusion-related alteration and regional metamorphism (i.e., Polat and Hofmann, 2003). This is supported by tight clusters of HFSE in normalized

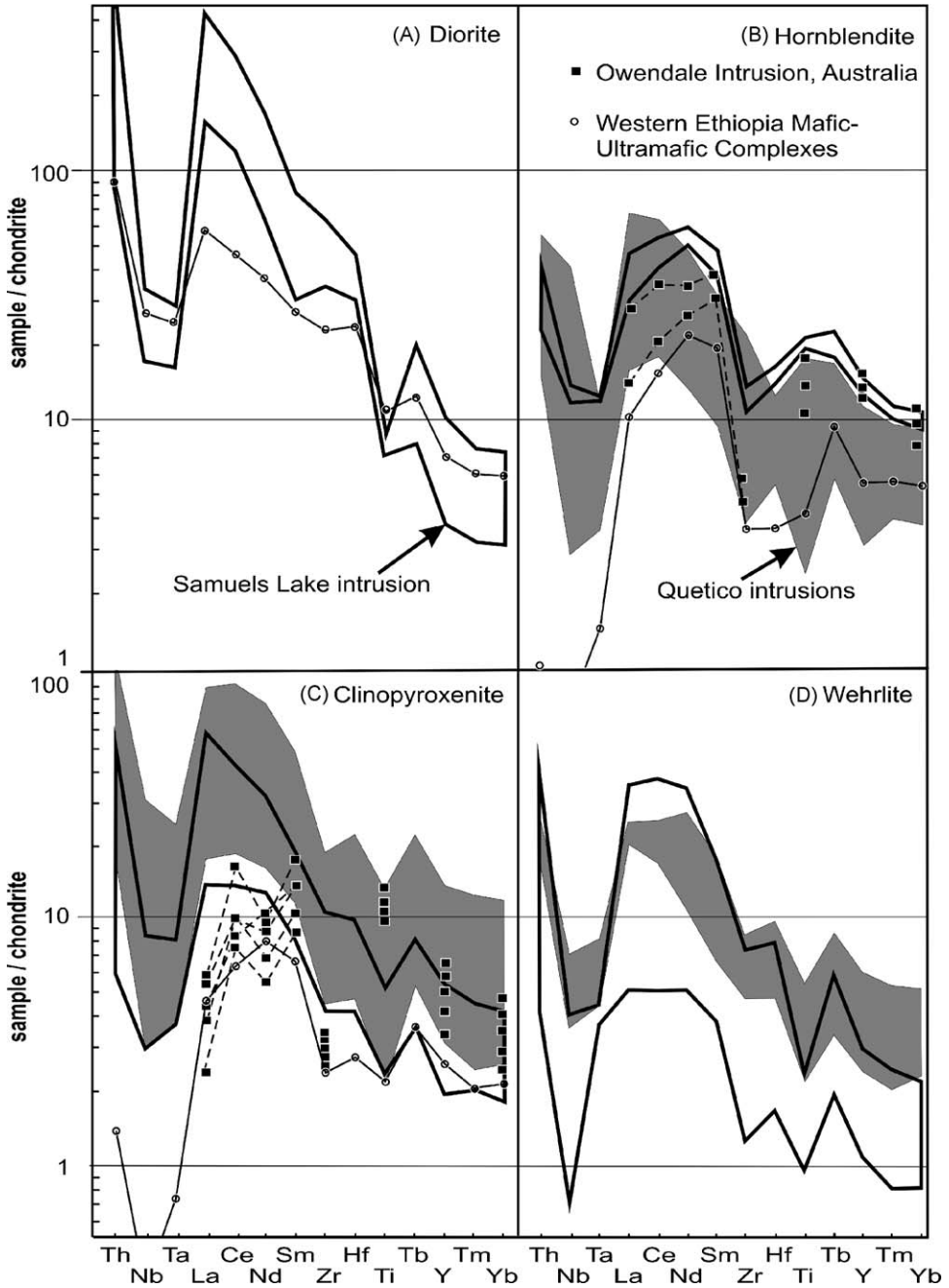

Fig. 6. Chondrite-normalized trace element plots of representative rocks of diorite (A), hornblendite (B), clinopyroxenite (C), and wehrite (D) of the Samuels Lake intrusion and Quetico Intrusions. The grey shaded areas show the compositional ranges of the Quetico Intrusions based on 32 representative samples from 10 intrusions (this study) and 30 samples from 7 intrusions determined by MacTavish (1999). The thick solid lines represent the data from the Samuels Lake intrusion (this study). The dashed black lines and filled symbols represent the rocks from the Owendale intrusion in New South Wales (Johan, 2002), and thin solid lines and open symbols represent rocks from various mafic–ultramafic complexes in western Ethiopia (Grenne et al., 2003). Several lines are not complete due to the lack of data. Chondrite values are McDonough and Sun (1995).

trace element patterns (Fig. 6). REE also display similar patterns except for minor scatter in light REE (Fig. 7), which is consistent with relatively high mobility of light REE in hydrothermal fluids compared to heavy REE.

4.2.2. *Parental magma of the Samuels Lake intrusion*

The nature of the parental magma is inferred from the bulk rock compositions of the intrusion due to the lack

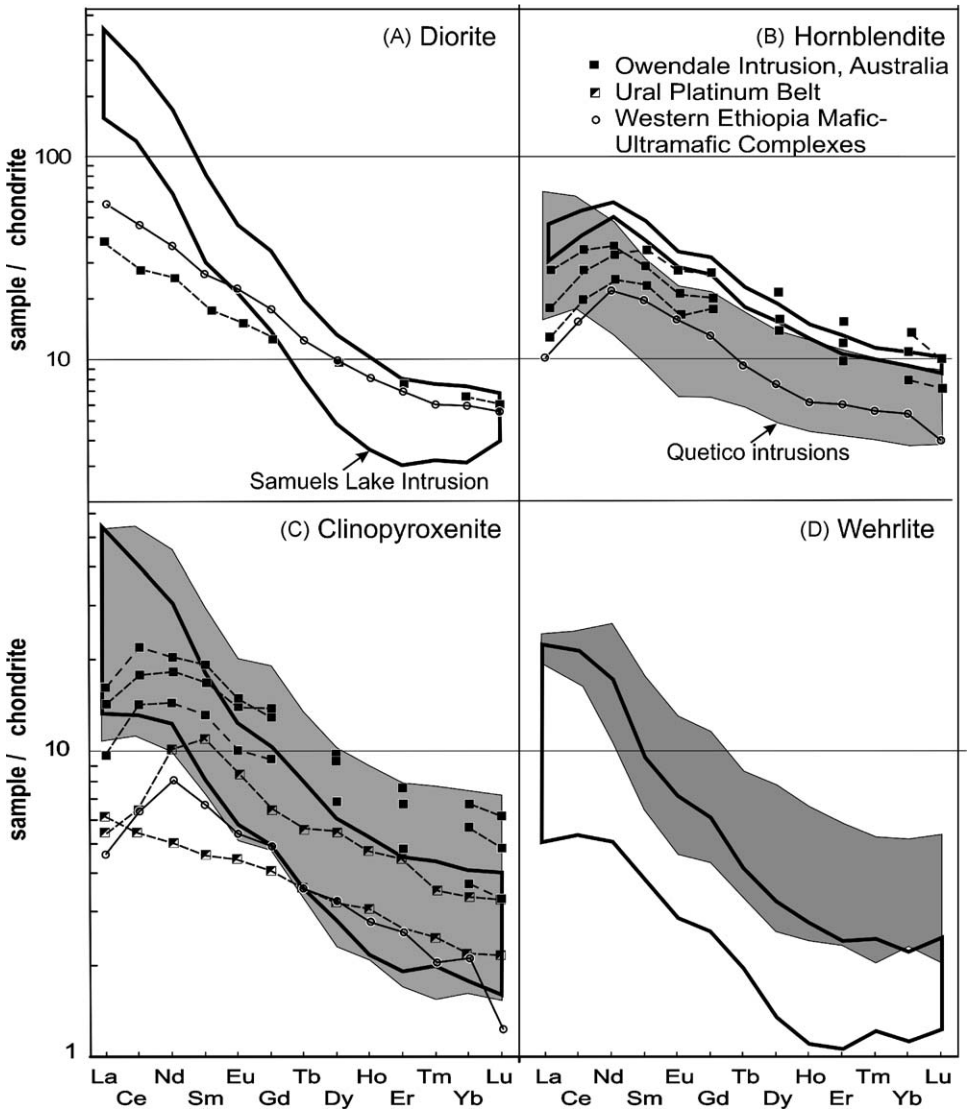

Fig. 7. Chondrite-normalized rare earth element patterns of diorite (A), hornblendite (B), clinopyroxenite (C), and wehrite (D) of the Samuels Lake intrusions (solid lines, this study) and the Quetico Intrusions (gray areas, this study). The dashed black lines and filled symbols represent the data from the Owendale intrusion, New South Wales (Johan, 2002) and the Ural Platinum Belt (Fershtater et al., 1997), thin solid lines and open symbols represent rocks from various mafic–ultramafic complexes in western Ethiopia (Grenne et al., 2003).

of chilled margins. The bulk rock compositions show the enrichment of large ion lithophile elements (LILE) and low HSFE, the so-called arc geochemical signature (Fig. 6). Although the concentrations of these trace elements in the parental melt may not represent those of the bulk rock compositions, their patterns should reflect those of the original parental magmas because ratios of these elements are not significantly modified during crystallization of olivine and clinopyroxene. Early crystallization of oxides may lower the concentrations of Nb and Ta in melt, but oxides are late phases and titanite occurs only as a secondary metamorphic product. This evidence combined with the lack of chromite and high Cr (up to 0.63 wt.%) in clinopyroxene indicate that oxides did not crystallize early in the parental magmas. Therefore, the trace element patterns of bulk rocks reflect those of the primitive melt.

Extensive crustal contamination can produce magmas with a trace element pattern with low Nb and Ta, but this possibility is not applicable for the Quetico Intrusions because of their overall high Mg and elevated Cr. Magmas get elevated contents of Si and Al during crustal contamination, and would not form olivine with high Mg and clinopyroxene with elevated Cr. Therefore, the arc

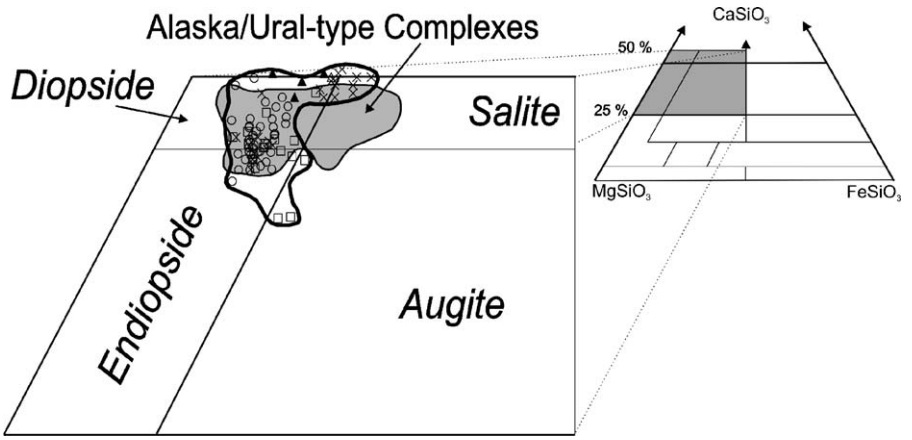

Fig. 8. Clinopyroxene composition of the Quetico Intrusions. The data from the Samuels Lake intrusion and other Quetico Intrusions are shown in symbols. They include 24 clinopyroxene grains from the Kawene, Abiwin, and North Elbow Lake intrusions. The plot includes the data from several Quetico Intrusions determined by MacTavish (1999). The grey field corresponds to the compositions of clinopyroxenes in Alaskan/Ural-type complexes; data from Irvine (1974), Rublee (1994) and Helmy and El Mahallawi (2003). Rock type symbols are: wehrite (circle), clinopyroxenite (square), hornblendite (triangle), and gabbro (×).

geochemical signature of the intrusions reflects that of the source mantle where fluid-mobile LILE are enriched by aqueous fluids discharged from slabs. The source for the Quetico Intrusion is a mantle wedge or an upper mantle that was once overlying subducting slabs.

The arc geochemical signatures of bulk rocks are consistent with clinopyroxene and hornblende compositions (Figs. 8–10). High concentrations of LILE in the parental magma are supported by abundant occurrence of primary hornblende and primary phlogopite/biotite throughout the intrusion. The abundance of these primary hydrous minerals indicates that the parental magma were not only rich in alkalis but also hydrous. The hydrous nature of the parental magma is supported by early crystallization of clinopyroxene. This is further supported by inferred high water contents of sulphide melt based on hydration of olivine in sulphide-rich wehrlite, abundant pegmatites, common brecciation around late dioritic dykes, and myrmekitic texture in diorite. A myrmekitic texture may form under a variety of conditions, but it is consis-

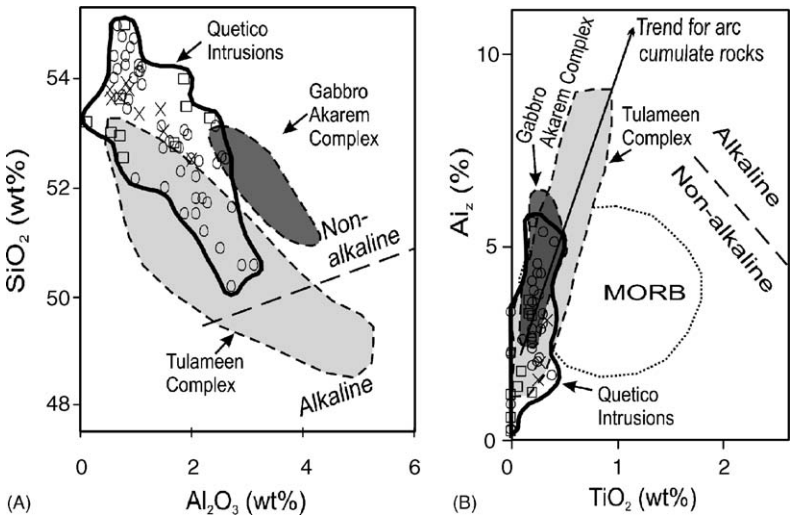

Fig. 9. Clinopyroxene compositions of the Samuels Lake intrusion and the Quetico Intrusions. The field of the Quetico Intrusions is based on the data from this study and includes the data of the Abiwin intrusion, determined by MacTavish (1999). The discrimination diagrams are after Le Bas (1962) where Alz refers to the percentage of Al in the tetrahedral sites ($100 \times {}^{IV}Al)/2$. The steep slope of the array in diagram B is characteristic of pyroxenes in hydrous arc magmas (Loucks, 1990). Data for the Tulameen Complex are from Rublee (1994) and the Gabbro Akarem Complex from Helmy and El Mahallawi (2003). The term non-alkaline by Le Bas (1962) includes rocks with tholeiitic, high-alumina, and calc-alkaline affinity. Rock type symbols are the same as those used in Fig. 8.

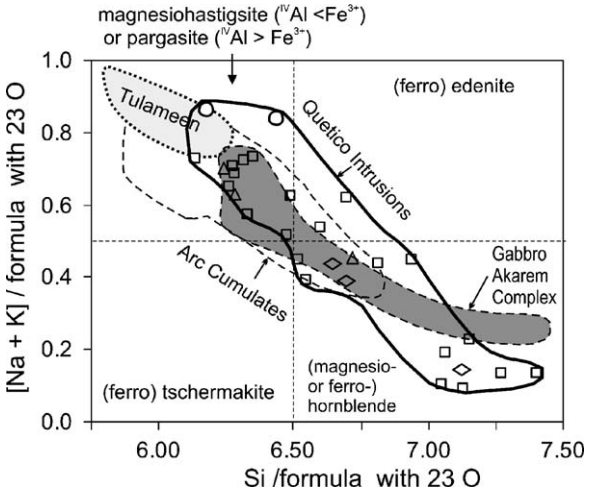

Fig. 10. Calcic amphibole compositions in the Quetico Intrusion versus those of Alaskan/Ural-type intrusions. Arc amphibole field is defined by Beard and Barker (1989). The data for the Quetico Intrusions field is from this study. Data for the Tulameen Complex by Rublee (1994) and the Gabbro Akarem Complex by Helmy and El Mahallawi (2003). Rock type symbols are the same as those used in Fig. 8 with the addition of diorite (flat diamonds). Compositional fields are after Leake et al. (1997).

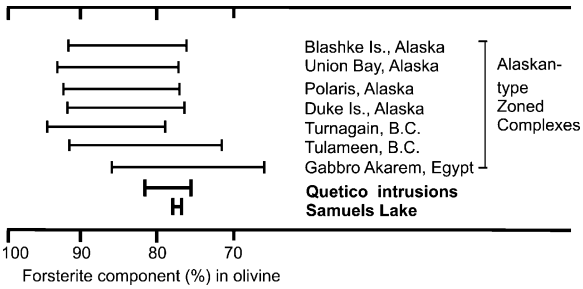

Fig. 11. Forsterite component of olivine from the Quetico Intrusions and Phanerozoic Alaskan/Ural type zoned complexes. Data sources: Quetico Intrusions (MacTavish, 1999; this study), Turnagain (Clark, 1980), Gabbro Akarem Complex (Helmy and Moggesie, 2001), Blashke Island (Himmelberg et al., 1986), Union Bay, Polaris, and Duke Island (Irvine, 1974, 1976), and the Tulameen Complex (Rublee, 1994).

tent with generation from water-rich magmas (Dymek and Schiffries, 1987).

5. Discussion

5.1. Comparison between Samuels Lake intrusion and mafic–ultramafic intrusions along the northern Quetico subprovince boundary

All mafic–ultramafic intrusions in the Quetico belt show similar characteristic features, including lithology, lithological zoning, textures, PGE mineralization, and similar mineral and bulk rock compositions. They all show fractionated REE with elevated light REE and little or no Eu anomalies (Fig. 7), elevated LILE, and apparent lows of Nb, Ta, and Ti (Fig. 6). Although alkali and alkali-earth elements were likely mobile, their consistently elevated concentrations and the occurrence of biotite or phlogopite indicate that they reflect the primary nature of the rocks (Fig. 6). The compositions of olivine, clinopyroxene, and hornblende are also similar among different intrusions (Figs. 8–11; Tables 1a–1c). These similarities suggest that the intrusions are cogenetic.

Ultramafic-mafic intrusions including three intrusions in the interior of the Quetico subprovince, display similar relationships to the host sedimentary rocks. The east-trending distribution of intrusions and the elongated shape of individual intrusions in the northern subprovince indicate that they likely intruded during the north–south transpressive deformation of D2. Metasedimentary country rocks contain numerous quartz segregation veins, especially in the northern subprovince, and several quartz veins cut the margin of the mafic–ultramafic intrusions, implying that they intruded prior to the peak M2 metamorphism. The intrusions along the northern boundary are considered to be ~2688 ± 4 Ma in age (Davis et al., 1990). This is consistent with the inferred age of the Samuels Lake intrusion, older than 2688 Ma + 6/−5 Ma, suggesting that these intrusions are likely to be contemporaneous.

PGE mineralization is accompanied by Cu–Ni–sulphides and is Pt-rich, with Pt/Pd ratios of around 1. Although Pt/Pd ratios of 1 are low compared to most Alaskan/Ural-type intrusions, the ratios are high compared to the surrounding Archean mafic–ultramafic intrusions, such as the Lac Des Iles Complex (~0.1) (Hinchey et al., 2005), Legris Lake Complex (~0.2; Pettigrew and Hattori, 2002), Grassy Portage Intrusion, and Bad Vermillion Lake intrusions (Poulsen and Hodgson, 1984).

5.2. Origin of the Quetico Intrusions

A variety of opinions have been proposed for the origin of the Quetico Intrusions. Williams (1989) proposed that they represent the remnants of mantle diapirs emplaced during the early sedimentation of the Quetico turbidites or tectonically dismembered ophiolites. MacTavish (1999) suggested that they are Archean examples of the Appinite suite of intrusions in the British Isles, which are closely associated with granitic plutons, and that the Quetico Intrusions formed during the two-mica granitic batholith emplacement in the centre

of the Quetico belt. Pirie (1978) and Watkinson and Irvine (1964) argued that they are cumulates of picritic tholeiitic magmas, which intruded into deeply buried sedimentary rocks. We reject the possible solid intrusion and tectonic emplacement of mantle rocks because the majority of intrusions show igneous contacts with the host sedimentary rocks, although some intrusions on the northern boundary have fault contacts. Even the narrow lenticular Mud Lake intrusion shows an igneous contact with the host sedimentary rocks. The compositions of the intrusions disprove the proposed origin as dismembered mantle peridotite.

A genetic relationship of these mafic–ultramafic intrusions to the peraluminous Quetico batholith is unlikely because of the age difference between the two. The rims of the Quetico Intrusions on the northern boundary are commonly intruded by quartz-rich aplite veins related to the Quetico batholiths of ~2670 Ma (Percival and Sullivan, 1988).

The lack of chilled margins in the Quetico Intrusions may support a possible feeder origin of the intrusions, because continuous flow of magma resorbs chilled margins. The parental magmas are interpreted to be high in MgO, greater than 10 wt.%, based on a calculation using MgO contents (18.0 wt.%; Table 1b) of clinopyroxene and the partition coefficient of Mg between clinopyroxene and melt (Hart and Dunn, 1993).

Clinopyroxene and hornblende grains plot in the fields of arc magmas (Figs. 8 and 10). These data indicate that the parental magmas were derived from mantle material that had undergone a previous melting event and was later enriched in LILE by fluids in a subduction setting. This proposed interpretation is supported by positive values of εNd (2690 Ma) from several mafic–ultramafic intrusions (+0.7 to +1.0; Lassen et al., 2001) along the northern subprovince boundary.

5.3. Comparison of Phanerozoic Alaskan/Ural-type and Quetico Intrusions

The Quetico Intrusions display many similarities with Phanerozoic Alaskan/Ural-type ultramafic–mafic intrusions (Table 3). Similarities between the two include the distribution, morphology, lithology, textures, mineralogy, mineral composition, bulk rock compositions, abundant hornblende, a common association with Cu–Ni–PGE mineralization, and the timing of intrusions relative to regional geodynamic activity. Alaskan/Ural-type intrusions were first described in southeastern Alaska and the Urals of Russia (Taylor, 1967; Taylor and Noble, 1969). In recent years, the definition of Ural-type intrusions has widened to include any large zoned ultramafic-mafic intrusions, such as the Konder and Inagli complexes in the Alden Shield of Siberia. As pointed out by Johan (2002), the intrusions in the Alden Shield are significantly different from traditionally defined Alaskan/Ural-type intrusions. In addition, the geodynamic setting and age of these intrusions in the Alden Shield is poorly known. Therefore, we follow the historical terminology of Taylor (1967), Taylor and Noble (1969), and Foley et al. (1997), that the Alaskan/Ural-type intrusions refer to ultramafic-mafic zoned intrusions in orogenic belts, and exclude large intrusions such as those in the Alden Shield.

Notable features of Alaskan/Ural-type intrusions include their relatively small size (generally 15–40 km^2), lithological zoning with ultramafic cores and gabbroic rims, their linear distribution along tectonic sutures, and common PGE mineralization (Table 3).

5.3.1. Intrusion morphology and mechanism

The Alaskan/Ural-type intrusions are generally small compared to other types of mafic–ultramafic igneous complexes (Foley et al., 1997). The Nizhni Tagil (70 km^2) and Tulameen complexes (~80 km^2) are considered to be exceptionally large Alaskan/Ural-type intrusions (Johan, 2002). Most are less than 5 km in diameter. This feature is similar to the Quetico Intrusions, which range from less than 100 m up to 5 km in diameter.

The contacts between country rocks and Alaskan/Ural-type intrusions are commonly faulted and sheared (Nixon et al., 1997), similar to the Quetico Intrusions (MacTavish, 1999; Pettigrew et al., 2000; this study), but they also show igneous contacts. When igneous contacts are present, both Alaskan/Ural-type and Quetico Intrusions display no chilled margins and no wide metamorphic aureoles (Nixon et al., 1997; Pettigrew et al., 2000). The lack of chilled margins have been explained by diapiric emplacement of differentiated cumulates (Irvine, 1974), semi-solidified magmas (Tistl, 1994; Helmy and El Mahallawi, 2003), of repeated injection of magmas as feeder pipes of overlying volcanic rocks (Murray, 1972; Conrad and Kay, 1984; Tistl, 1994; Tistl et al., 1994).

For the Quetico Intrusions, a variety of models have also been proposed for their emplacement, including diapiritic solid intrusions and tectonic emplacement (Williams, 1989), and solid emplacement of cumulates (Pirie, 1978).

5.3.2. Lithology

The Alaskan/Ural-type intrusions are characterized by concentric zoning of lithologies, with a gabbroic

Table 3
Comparison between Alaskan/Ural-type and Quetico Intrusions

	Alaskan/Ural-type Intrusions	Quetico Intrusions
Age	Mostly Phanerozoic	Late Archean
Distribution	Clusters of intrusions form long linear arrays along major tectonic boundaries in orogenic belts	Clusters of intrusions form a linear array parallel to the Quetico–Wabigoon subprovince boundary. It extends southwest to the centre of the subprovince
Geological setting	Close to the end of subduction, prior to accretion-collision	Close to the end of subduction, prior to accretion-collision
Size	Most are small in size (<4 km)	Most are small in size (<3.0 km)
Morphology and zoning	Crude concentric zoning of lithologies grading from olivine-rich ultramafic cores to mafic rims Lack of chilled margin Little or no metamorphic aureole	Crude concentric lithological zonation with olivine-bearing ultramafic cores grading into mafic rims Lack of chilled margin Little or no metamorphic aureole
Sequence of intrusion	Gabbroic and dioritic rocks intrude late	Late intrusion of dioritic rocks
Lithology	Abundant hornblendite and clinopyroxenite Minor dioritic and syenitic rocks	Abundant hornblendite and clinopyroxenite Minor dioritic and syenitic rocks
Lithological zoning	Olivine-rich core phases (dunite)	Olivine-bearing ultramafic rocks (wehrite) in cores
Pegmatites	Common occurrence of hornblende-bearing pegmatites	Common occurrence of hornblende-bearing pegmatites
Textures	Poikilitic textured hornblende in clinopyroxenite, common occurrence of mafic pegmatites	Poikilitic textured hornblende in clinopyroxenite, common occurrence of mafic pegmatites
Mineralogy	Abundant clinopyroxene, hornblende. Common occurrence of secondary magnetite Essential lack of orthopyroxene	Abundant clinopyroxene, hornblende. Common occurrence of secondary magnetite Essential lack of orthopyroxene
Chromite	Common occurrence of chromite in dunite	Chromium does not form oxides. Instead, Cr is in clinopyroxene
Mineral chemistry	High Mg olivine, diopsidic clinopyroxene, phlogopitic mica. Amphibole is calcic showing, a wide range in composition	High Mg olvine, diposidic clinopyroxene, phlogopitic mica Amphibole is calcic showing a wide range in composition
Bulk rock geochemistry	High LILE and low HFSE Fractionated REE with no Eu anomalies	High LILE and low HFSE Fractionated REE with no Eu anomalies
PGE mineralization	PGE mineralization in olivine-rich cores (dunite) associated with chromite or Cu–Ni sulphides	PGE mineralization in olivine-rich cores (werhlite) associated with Cu–Ni sulphides
Parental magmas	Hydrous, elevated LILE and low HFSE, no Eu anomalies	Hydrous, elevated LILE and low HFSE, no Eu anomalies
Examples	Union Bay, Goodnews Bay, and Salt Chuck intrusions in Alaska; Lunar Creek, Johanson Lake, Menard Creek, Tulameen, Wrede Creek, and Turnagain complexes in British Columbia, Canada; Alto Condoto complex in Colombia; Owendale in Australia; Joubdo, Tulu Dimtu, Gabbro Akarem complexes in Ethiopia; Nizhny Tagil in Russia	Kawene Lake, Samuels Lake, Chief Peters, Abiwin, Plateau Lake, North Elbow, Mud Lake, Nym Lake, Eva Lake, Stawson Lake, Red Horse Creek intrusions

outer rim grading inward to olivine-rich cores (Murray, 1972; Irvine, 1974; Taylor and Noble, 1969; Nixon et al., 1997; Foley et al., 1997). Cores consist of dunite, wehrite, olivine clinopyroxenite, clinopyroxenite, hornblende clinopyroxenite, clinopyroxene hornblendite, or hornblende- and/or clinopyroxene-bearing gabbro/diorite. Minor feldspar-bearing rocks, such as diorite, monzonite, monzodiorite, syenite, and pegmatites are late and these dykes cut earlier rocks. Examples include late coarse-grained hornblende gabbro dykes in the Owendale complex of New South Wales, Australia (Johan, 2002), as well as in the El Chacao and Cerro Pelon intrusions of northern Venezuela (Murray, 1972) and hornblende-pegmatite dykes in the Judd Harbor complex in Alaska (Irvine, 1974, 1976). The Quetico Intrusions share many of these features such as crude concentric zoning with gabbro, hornblendite and clinopyroxenitie rims grading into olivine-rich wherlite

cores, as well as characteristic late phases such as diorite dykes and plugs.

Both Alaskan/Ural-type intrusions and Quetico Intrusions contain abundant clinopyroxene, olivine, and hornblende with essentially no orthopyroxene (Nixon et al., 1997; Foley et al., 1997; Irvine, 1974; MacTavish, 1999; Pettigrew et al., 2000). Poikilitic textures are common in Alaskan/Ural-type intrusions, especially in hornblende-rich lithologies (Murray, 1972; Nixon et al., 1997). Large (up to 5 cm) poikilitic clinopyroxene and hornblende and enclosing clinopyroxene ± olivine is also characteristic of the Quetico Intrusions, giving them a distinctive appearance in the field (Fig. 5B). Pegmatitic hornblende + plagioclase dykes and veins are also characteristic of both the Alaskan/Ural-type (Irvine, 1974; Murray, 1972; Tistl et al., 1994) and the Quetico intrusions (MacTavish, 1999; Pettigrew et al., 2000).

5.3.3. Bulk rock and mineral compositions

Similar to the Quetico Intrusions, Akaskan/Ural-type intrusions display elevated LILE with low Nb, Ta, and Ti (Johan, 2002; Tistl et al., 1994; Nixon et al., 1997; Grenne et al., 2003) (Fig. 6). This evidence indicates the derivation of their parental magmas from a depleted mantle source that has undergone metasomatism in a subduction setting.

The Quetico and Alaskan/Ural-type intrusions display negatively sloped REE patterns with no Eu anomalies (Fig. 7). The lack of Eu anomalies is consistent with suppressed crystallization of plagioclase in the parental magmas in water-rich melt (Gaetani et al., 1993). It may also reflect the oxidized nature of the parental magmas, because all REE including Eu are trivalent in an oxidized melt.

Olivine is Mg-rich (Fig. 11) and clinopyroxene is diopsidic in both Quetico and Alaskan/Ural-type intrusions (Fig. 8). Clinopyroxene in Alaskan/Ural-type intrusions are also characterized by low Ti contents and low Al in tetrahedral sites (Loucks, 1990; Helmy and Moggesie, 2001; Helmy and El Mahallawi, 2003), similar to the Quetico Intrusions (Fig. 9). Even amphiboles from both groups of intrusions show a similar composition and compositional variations (Fig. 10). One notable difference between the two is the lack of chromite in the Quetico Intrusions. Alaskan/Ural-type intrusions commonly contain chromite in dunite, whereas Cr in Quetico Intrusions is bound in silicate minerals, mostly in clinopyroxene (up to 0.63 wt.% Cr_2O_3 in the Samuels Lake intrusion and up to 1.0 wt.% Cr_2O_3 in other Quetico Intrusions; Table 1b). It is not certain what caused the incorporation of Cr in clinopyroxene in Archean intrusions.

5.3.4. Cu–Ni–PGE mineralization

Alaskan/Ural-type intrusions and associated placers have historically been an important source of Pt (Johan, 2002). The mineralization is associated either with chromite or Cu–Ni sulphides in the olivine-rich cores of the intrusions (Nixon et al., 1997; Johan, 2002). Examples of chromite-associated PGE mineralization include the Tulameen complex in British Columbia (Nixon et al., 1997), the Goodnews Bay complex in Alaska (Mertie, 1976), and the Nizhni Tagil and Konder complex in the Urals (Johan, 2002). Examples with Cu–Ni sulphide-associated PGE mineralization include the Salt Chuck intrusion in Alaska (Loney and Himmelberg, 1992), Gabbro Akarem in Egypt (Helmy and Moggesie, 2001), and the Turnagain intrusion in British Columbia (Scheel et al., 2005). The latter examples are comparable to the Cu–Ni–PGE mineralization in the wehrite cores of the Quetico Intrusions.

5.3.5. Parental magmas

The parental magmas for the Alaskan/Ural-type intrusions were picritic and hydrous (Loucks, 1990; Loney and Himmelberg, 1992), with arc tholeiite affinity (Murray, 1972; Conrad and Kay, 1984; Tistl, 1994; Helmy and El Mahallawi, 2003). The Quetico Intrusions also formed from Mg-rich hydrous magmas with strong arc geochemical signatures.

5.4. Geodynamic settings

5.4.1. Geodynamic setting of Alaskan/Ural-type intrusions

Alaskan/Ural-type intrusions are restricted to late-Precambrian and Phanerozoic orogenic belts, such as those in the Cordillera of North and South America (Taylor, 1967; Irvine, 1974; Tistl, 1994), Urals (Fershtater et al., 1997), New South Wales (Johan, 2002), and along the East African orogenic zone in western Ethiopia (Grenne et al., 2003). These intrusions all form linear arrays along major tectonic sutures and intruded during terrane accretion, following the subduction of intervening oceanic crust. For example, Ural-type intrusions in Russia occur east along the Main Uralian Fault, which is the major suture between arc terranes to the east and the East European continent to the west; the Ural-type mafic–ultramafic complexes intruded during accretion of arc terranes to the continent (Ayarza et al., 2000). A similar geodynamic setting has been proposed for Alaskan-type intrusions in Alaska. They occur in the western margin of the North America continent where arcs and micro-continents accreted from the west. Based on a detailed structural study of the Duke Island complex

in Alaska, Saleeby (1992) suggested that Alaskan-type intrusions likely intruded during the closure of the intra-arc basin, which corresponds the final phase of accretion of the Alexander terrane to North America (Foley et al., 1997). Recent studies of western Ethiopia illustrate a similar tectonic setting for the mafic–ultramafic complexes, which occur along a major shear deformation zone, the Baruda fault, and formed from a mantle wedge metasomatized during the subduction of Mozambique ocean crust before the oblique collision of two continents (Worku and Schandelmeier, 1996; Grenne et al., 2003).

5.4.2. Geodynamic setting of the Quetico Intrusions

The distribution and geodynamic setting of the Quetico Intrusions are similar to those of the Alaskan/Ural-type intrusions. The Quetico Intrusions form an array along the boundary between the Quetico belt and the Wabigoon subprovince, which is the suture of the Quetico fore-arc prism and the continental arc of the Wabigoon subprovince to the north (e.g., Williams, 1991; Valli et al., 2004).

The Archean Superior Province formed through accretion of microcontinents and arcs to the north through subduction of intervening oceanic crust (e.g., Williams, 1991; White et al., 2003). Before 2700 Ma, the Wabigoon subprovince was the southern margin of the proto-Superior Province and overlain by a continental arc due to northward subduction of intervening oceanic crust beneath the southern margin. During active subduction, sediments accumulated in the fore-arc prism forming the Quetico subprovince (Williams, 1991; Valli et al., 2004). The sedimentation was continuous until ~2690 Ma based on the youngest detrital zircon age of 2688.5 ± 1 Ma in the Quetico subprovince (Zaleski et al., 1999); formation of the accretionary prism ended when the Wawa arc accreted to the Quetico and Wabigoon subprovinces. The age of the youngest detrital zircon is very similar to the inferred age of the Quetico Intrusions, ~2690 Ma (Davis et al., 1990). This suggests that the Quetico intrusions intruded in the active fore-arc prism or shortly after the cessation of sedimentation. In either case, the Quetico Intrusions represent the final subduction-related magmatism prior to the juxtaposition of the Wawa arc with the Wabigoon subprovince.

The accretion of the Wawa arc to the Wabigoon subprovince is considered to have been oblique, based on the predominant dextral sense of shear deformation and suture zones (e.g., Tabor and Hudleston, 1991; Williams, 1991). Oblique convergence of plates likely causes the descending subducting slabs to become steep (e.g., Fossen and Tikoff, 1998). Steep oblique subduction is commonly accompanied by mafic magmatism in front of the slabs or near the areas of the breaking slabs due to the heat provided by the upwelling asthenospheric mantle. Therefore, the generation of primitive parental magmas for the Quetico Intrusions is expected following the approach of the Wawa arc to the Quetico–Wabigoon subprovinces. Considering the arc geochemical signatures of the parental magmas, partial melting likely took place in the mantle wedge in front of the steepened slab. The proposed interpretation is consistent with the NE-SW orientation of the Quetico Intrusions, which is parallel to the strike of the Wawa arc before its juxtaposition to the western Superior Province. The mafic magmatism was short lived because this geodynamic setting was transient before the Wawa arc accreted to the Quetico and Wabigoon subprovinces.

6. Summary

Identification of the Samuels Lake, Stawson Lake, and Red Horse Creek intrusions as part of the Quetico Intrusions has extended the array 80 km further to the southwest. The intrusions now form an overall NE-SW trending array over 125 km long, starting from the northern subprovince boundary towards the southwestern across the Quetico subprovince. The Samuels Lake intrusion in the centre of the subprovince intruded at ~2688 + 6/−5 Ma, which is similar to the inferred age, ~2690 Ma, of the intrusions along the northern subprovince boundary, confirming their contemporaneous igneous activity.

The Quetico Intrusions have many similarities to Alaskan/Ural-type complexes along Phanerozoic orogenic belts. These include the relatively small size of individual intrusions, linear arrays of intrusions along major sutures, concentric zoning from olivine-rich cores to the intrusion, arc-geochemical signatures, similar mineralogy, and accompanying PGE mineralization. The geodynamic setting is also similar for both Alaskan/Ural-type intrusions and the Quetico Intrusions; they all intruded during accretion of arcs to continents. The Quetico Intrusions most likely were emplaced during the very early stage of accretion of the Wawa arc to the Quetico–Wabigoon subprovinces to the north. Oblique accretion of the Wawa arc resulted in a steepened slab and upwelling of the asthenospheric mantle. The heat allowed high degrees of partial melting in the mantle wedge for the formation of the parental magmas of the Quetico Intrusions.

Acknowledgments

We thank ProAm Exploration Corporation and Starcore Resources Ltd. for their support during fieldwork, and for providing diamond drill core samples and company reports. W.C. Hood, formerly of ProAm Exploration Corporation, was helpful throughout the study. We thank V. McNicoll of the Geological Survey of Canada for allowing us to use unpublished U–Pb ages of our zircon and titanite samples in this manuscript, B. Lassen for her assistance during fieldwork, P. Jones for his help with electron microprobe analysis, R. Hartree for the XRF analyses, M. Wilk-Alemany for analysis of PGEs, and John Percival for facilitating the U–Pb age analysis of samples at the Geological Survey of Canada and suggestions on an earlier draft of this manuscript. Lithoprobe and NSERC Discovery grants to KHH provided financial support for this project. We also thank two anonymous journal reviewers for their constructive comments.

References

Ayarza, P., Brown, D., Alvarez-Marron, J., Juhlin, C., 2000. Contrasting tectonic history of the arc-continent suture in the southern and middle Urals: implications for the evolution of the orogen. J. Geol. Soc. Lond. 157, 1065–1076.

Beard, J.S., Barker, F., 1989. Petrology and tectonic significance of gabbros, tonalities, shoshonites and anorthosites in a late Paleozoic arc-root complex in the Wrangellia terrane, southern Alaska. J. Geol. 97, 667–683.

Blackburn, C.E., John, G.W., Ayer, J., Davis, D.W., 1991. Wabigoon subprovince. Geology of Ontario. Ontario Geological Survey Specification, Part 1, vol. 4, pp. 303–381.

Clark, T., 1980. Petrology of the Turnagain ultramafic complex, northwestern British Colombia. Can. J. Earth Sci. 17, 744–757.

Conrad, W.K., Kay, R.W., 1984. Ultramafic and mafic inclusions from Adak Island: crystallization history, and implications for the nature of primary magmas and crustal evolution in the Aleutian Arc. J. Petrol. 25, 88–125.

Davis, D.W., Pezzutto, F., Ojakangas, R.W., 1990. The age and provenance of metasedimentary rocks in the Quetico Subprovince, Ontario, from single zircon analyses: implications for Archean sedimentation and tectonics in the Superior Province. Earth Planet. Sci. Lett. 99, 195–205.

Davis, D.W., Poulsen, K.H., Kamo, S.L., 1989. New insights into Archean crustal development from geochronology in the Rainy Lake area, Superior Province, Canada. J. Geol. 97, 379–398.

Dymek, R.F., Schiffries, C.M., 1987. Calcic myrmekite: possible evidence for the involvement of water during the evolution of andesine anorthosite from St.-Urbain, Quebec. Can. Min. 25, 291–319.

Fershtater, G.B., Montero, P., Borodina, N.S., Pushkarev, E.V., Smirnov, V.N., Bea, F., 1997. Uralian magmatism: an overview. Tectonophysics 276, 87–102.

Foley, J.P., Light, T.D., Nelson, S.W., Harris, R.A., 1997. Mineral occurrences associated with mafic–ultramafic and related alkaline complexes in Alaska. Econ. Geol. Monogr. 9, 396–449.

Fossen, H., Tikoff, B., 1998. Extended models of transpression and transtension, and application to tectonic setting. In: Holdsworth, R.E., Strachan, R.A., Dewey, J.F. (Eds.), Continental Transpressional and Transtensional Tectonics, vol. 135. Geological Society of London, pp. 15–33 (Special Publication).

Francis, R.D., 1990. Sulfide globules in mid-ocean ridge basalts (MORB), and the effect of oxygen abundance in Fe–S–O liquids on the ability of those liquids to partition metals from MORB and komatiite magmas. Chem. Geol. 85, 199–213.

Gaetani, G.A., Grove, T.L., Bryan, W.B., 1993. The influence of water on the petrogenesis of subduction-related igneous rocks. Nature 365, 332–334.

Geological Survey of Canada and Ontario Department of Mines, 1965a. Quetico, Ontario, Geophysics Map 7090G (scale 1:250,000).

Geological Survey of Canada and Ontario Department of Mines, 1965b. Quetico, Ontario, Geophysics Map 7091G (scale 1:253,440).

Grenne, T., Pedersen, R.B., Bjerkgård, T., Braathen, A., Selassie, M.G., Worku, T., 2003. Neoproterozoic evolution of Western Ethiopia; igneous geochemistry, isotope systematics and U–Pb ages. Geol. Mag. 140, 373–395.

Guillot, S., Hattori, K.H., de Sigoyer, J., 2000. Mantle wedge serpentinization and exhumation of eclogites: insights from eastern Ladakh, NW Himalaya. Geology 28, 199–202.

Hart, S.R., Dunn, T., 1993. Experimental Cpx/melt partitioning of 24 trace elements. Contrib. Mineral. Petrol. 113, 1–8.

Hattori, K., Percival, J.A., 1999. Archean carbonate-bearing alkaline igneous complexes of the western Quetico metasedimentary belt, Superior Province, Ontario. Curr. Res. Geol. Surv. Can. 1999-C, 221–231.

Helmy, H.M., Moggesie, A., 2001. Gabbro Akarem, Eastern Desert, Egypt: Cu–Ni–PGE mineralization in a concentrically zoned mafic–ultramafic complex. Min. Deposita 36, 58–71.

Helmy, H.M., El Mahallawi, M.M., 2003. Gabbro Akarem mafic–ultramafic complex, Eastern Desert, Egypt: a late Precambrian analogue of Alaskan-type Complexes. Mineral. Petrol. 77, 85–108.

Himmelberg, G.R., Loney, R.A., Craig, J.T., 1986. Petrogenesis of the ultramafic complex of the Blashke Islands, southeastern Alaska. U.S. Geol. Surv. Bull. 1662, 14.

Hinchey, J.G., Hattori, K.H., Lavigne, M., 2005. Geology, petrology, and controls on PGE mineralization of the Southern Roby and Twilight Zones, Lac des Iles mine, Canada. Econ. Geol. 100, 43–61.

Irvine, T.N., 1974. Petrology of the Duke Island ultramafic complex southern Alaska. Geol. Soc. Am. Memoir 138, 240.

Irvine, T.N., 1976. Alaskan-type ultramafic-gabbro bodies in the Aiken Lake, McConnel Creek, and Toodagoone map-areas. Geol. Surv. Can. Paper 76-1A, pp. 76–81.

Johan, Z., 2002. Alaskan-type complexes and their platinum-group element mineralizaiton. In: Cabri, L.J. (Ed.), Geology, Geochemistry, Mineralogy and Mineral Beneficiation of Platinum-group Elements, vol. 54. Can. Inst. Min. Metall. Sp., pp. 669–719.

Lassen, B., Hattori, K., Percival, J., 2001. Nd and Pb isotope geochemistry for Neoarchean alkaline intrusions in the western Superior Province, Canada. EOS Trans. Am. Geophys. Union Abst. 32, 1028.

Leake, B.E., Wooley, A.R., Arps, C.E.S., Birch, W.D., Gilbert, M.C., Grice, J.E., Hawthorne, F.C., Kato, A., Kisch, H.J., Krivovichev, V.G., Linthout, K., Laird, J., Mandarino, J.A., Maresch, W.V., Nickel, E.H., Rock, N.M.S., Schumacher, J.C., Smith, D.C., Stephenson, N.C.N., Ungaretti, L., Whittaker, E.J.W., Youzhi, G., 1997. Nomenclature of amphiboles: Report of the subcomiittee on amphiboles of the international mineralogical association.

Commission on new minerals and mineral names. Can. Min. 35, 219–246.

Le Bas, M.J., 1962. The role of aluminum in igneous clinopyroxenes with relation to their parentage. Am. J. Sci. 260, 267–288.

Loney, R.A., Himmelberg, G.R., 1992. Petrogenesis of the Pd-rich intrusion at Salt Chuck. Prince of Wales Island: an early Paleozoic Alaskan-type ultramafic body. Can. Min. 30, 1005–1022.

Loucks, R.R., 1990. Discrimination of ophiolitic from nonophiolitic ultramafic-mafic allochthons in orogenic belts by the Al/Ti ration in clinopyroxene. Geology 18, 346–349.

MacTavish, A.D., 1999. The mafic–ultramafic intrusions of the Aitikokan-Quetico area northwestern Ontario. Ont. Geol. Surv. Open File Rep. 5997, 127.

McDonough, W.F., Sun, S., 1995. The composition of the Earth. Chem. Geol. 120, 223–253.

Mertie, J.B., Jr., 1976. Platinum deposits of the Goodnews Bay District, Alaska. U.S. Geol. Survey, Prof. Paper 938, 42 pp.

Murray, C.G., 1972. Zoned ultramafic complexes of the Alaskan type: feeder pipes of andesitic volcanoes. Geol. Soc. Am. Memoir 132, 313–335.

Nixon, G.T., Hammack, J.L., Ash, C.H., Cabri, L.J., Case, G., Connelly, J.N., Heaman, L.M., Laflamme, J.H.G., Nuttall, C., Paterson, W.P.E., Wong, R.H., 1997. Geology and platinum-group-element mineralization of Alaskan-type ultramafic–mafix complexes in British Columbia. In: British Columbia Ministry of Employment and Investment, Energy and Mines Division, Bulletin, p. 93.

Percival, J.A., Sullivan, R.W., 1988. Age constraints on the evolution of the Quetico Belt, Superior Province, Ontario. Radiogenic and isotopic studies, Report 2, Geological Survey of Canada Paper 88-2, pp. 97–107.

Pettigrew, N.T., Hattori, K.H., Percival, J.A, 2000. Samuels Lake intrusion, Northwestern Ontario: a late Archean Cu–Ni–PGE bearing mafic–ultramafic complex in the western Quetico Subprovince. Geol. Surv. Can. Curr. Res. 2000-C20, 8 pp.

Pettigrew, N.T., Hattori, K.H., 2002. Palladium–copper–rich PGE mineralization in the Legris Lake mafic ultramafic complex, western Superior Province of Canada. Trans. Inst. Min. Metall. 111, B46–B57.

Pirie, J., 1978. Geology of the Crooked Pine lake Area District of Rainy River. Ont. Geol. Survey Rep. 179, 20–28.

Polat, A., Hofmann, A.W., 2003. Alteration and geochemcial patterns in the 3.7–3.8 Ga Isua greenstone belt, West Greenland. Precambrian Res. 126, 197–218.

Poulsen, K.H., Hodgson, C.J., 1984. Mineralization associated with Archean gabbro-anorthosite intrusions in the Rainy Lake area, northwestern Ontario, vol. 34, Can. Inst. Min. Metall. Sp, pp. 329–344.

Rublee, V.J., 1994. Chemical petrology, mineralogy and structure of the Tulameen Complex, Princeton area, British Colombia. Unpublished M.Sc. thesis. University of Ottawa, Canada. p. 179.

Saleeby, J.B., 1992. Age and tectonic setting of the Duke Island ultramafic intrusion, southeast Alaska. Can. J. Earth Sci. 29, 506–522.

Scheel, J.E., Nixon, G.T., Scoates, J.S. 2005. New Observations on the geology of the turnagain alaskan-type ultramafic intrusive suite and associated Ni–Cu–PGE mineralization, British Columbia. British Columbia Geol. Surv. Geol. Fieldwork 2004. Paper 2005-1.

Tabor, J.R., Hudleston, P.J., 1991. Deformation at an Archean Subprovince boundary, northern Minnesota. Can. J. Earth Sci. 28, 292–307.

Taylor Jr., H.P., Noble, J.A., 1969. Origin of magnetite in the zoned ultramafic complexes of southeastern Alaska. In: Wilson, H.D.B. (Ed.), Magmatic Ore Deposits. Econ. Geol. Monographs, vol. 4, pp. 209–230.

Taylor Jr., H.P., 1967. The zoned ultramafic complexes of southeastern Alaska. In: Wyllie, P.J. (Ed.), Ultramafic and Related Rocks. Wiley, New York, pp. 97–121.

Tistl, M., 1994. Geochemistry of platinum-group elements of the zoned ultramafic Alto Condoto Complex, Northwest Colombia. Econ. Geol. 89, 158–167.

Tistl, M., Burgath, K.P., Hohndorf, A., Kreuzer, H., Munoz, R., Salinas, R., 1994. Origin and emplacement of Tertiary ultramafic complexes in northwest Colombia: evidence from geochemistry and K–Ar, Sm–Nd and Rb–Sr isotopes. Earth Planet. Sci. Lett. 126, 41–59.

Valli, F., Guillot, S., Hattori, K.H., 2004. Source and tectonometamorphic evolution of mafic and pelitic metasedimentary rocks from the central Quetico metasedimentary belt, Archean Superior Province of Canada. Precambrian Res. 132, 155–177.

Watkinson, D.H., Irvine, T.N., 1964. Peridotitic intrusions near Quetico and Shebandowan, northwestern Ontario: a contribution to the petrology and geochemistry of ultramafic rocks. Can. J. Earth Sci. 1, 63–98.

White, D.J., Musacchio, G., Helmstaedt, H.H., Harrap, R.M., Thurston, P.C., Vander Verlden, A., Hall, K., 2003. Images of a lower-crustal oceanic slab: Direct evidence for tectonic accretion in the Archean western Superior province. Geology 31, 997–1000.

Williams, H.R., 1989. Evolution of an Archean Subprovince boundary: a sedimentological and structural study of part of the Wabigoon–Quetico boundary in northern Ontario. Can. J. Earth Sci. 26, 1013–1026.

Williams, H.R., 1991. Quetico Subprovince. Geology of Ontario, Part 1, vol. 4. Ont. Geol. Survey, Sp, pp. 383–403.

Worku, H., Schandelmeier, H., 1996. Tectonic evolution of the Neoproterozoic Adola Belt of southern Ethiopia; evidence for a Wilson Cycle process and implications for oblique plate collision. Precambrian Res. 77, 179–210.

Wykes, J.L., Mavrogenes, J.A., 2005. Hydrous sulfide melting: Experimental evidence for the solubility of H_2O in sulfide melts. Econ. Geol. 100, 157–164.

Zaleski, E., van Breemen, O., Peterson, V.L., 1999. Geological evolution of the Manitouwadge greenstone belt ad Wawa-Quetico Subprovince boundary, Superior Province, Ontario, constrained by U–Pb zircon dates of supracrustal and plutonic rocks. Can. J. Earth Sci. 36, 945–966.